CHEMISTRY OF MATERIALS

pubs.acs.org/cm

Article

Expanding the Versatility of Dynamic Covalent Hydrogels with Static Covalent Spot-Welding

Michelle S. Huang,[¶] Renato S. Navarro,[¶] Lucia G. Brunel, Narelli de Paiva Narciso, Giselle Aviles Rodriguez, Neil J. Baugh, Julien G. Roth, Sarah M. Hull, Kelsea M. Hubka, and Sarah C. Heilshorn*

Cite This: *Chem. Mater.* 2025, 37, 9758−9774

Read Online

ACCESS | Metrics & More | Article Recommendations | Supporting Information

ABSTRACT: Hydrogels cross-linked through dynamic covalent chemistry (DCC) can mimic the viscoelastic properties of native biological tissues; however, these materials often suffer from rapid erosion, greatly limiting their application in biological studies. To address this challenge, we developed a DCC hydrogel with enhanced stability by sparsely distributing static covalent bonds, termed "spot-welds," throughout the network. These spot-welds served as anchor points to prevent polymer erosion and significantly improved gel stability without compromising viscoelasticity. Specifically, our single-network system (termed HELP) consisted of two recombinant biopolymers, hyaluronic acid (HA) and an engineered elastin-like protein (ELP), each modified to cross-link through both dynamic hydrazone bonds and static strain-promoted azide−alkyne cycloaddition (SPAAC) bonds. Gels with and without sparsely distributed spot-welds had similar stiffness ($G' \sim 800$ Pa), stress relaxation rates ($\tau_{1/2} \sim 6000$ s), and shear-thinning behavior, resulting in gels that were viscoelastic and extrudable through a 3D printing syringe. Importantly, the spot-welds significantly improved gel stability, with DCC-only gels suffering complete erosion by day 4, while spot-welded gels remained stable for at least 14 days. This combination of enhanced gel stability with viscoelastic mechanics enabled the 3D culture and maturation of human stem cell-derived cardiomyocytes. While elastic control gels resulted in loss of cardiomyocyte phenotype, the spot-welded viscoelastic gels supported cardiomyocyte spreading, spontaneous beating, and expression of α-actinin and troponin T. In summary, sparsely distributing static cross-links on each biopolymer within a dynamic covalent network results in an injectable and printable single-network hydrogel with viscoelastic mechanics and significantly enhanced stability, supporting 3D cardiomyocyte culture and maturation.

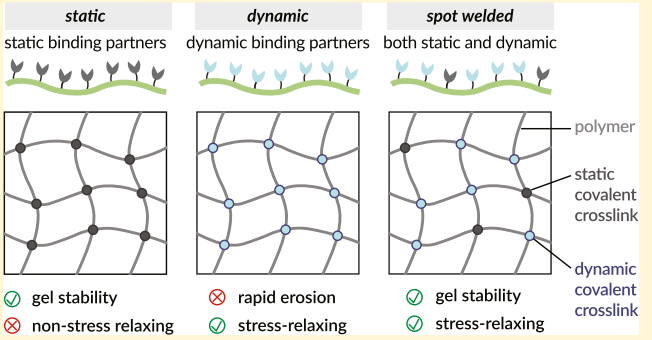

INTRODUCTION

Hydrogels are attractive platforms for tissue engineering as they are able to mimic the biochemical and biomechanical properties of the native extracellular matrix (ECM).[1] Static cross-linking strategies are often employed to form a stable and robust hydrogel network, but hydrogels formed through static covalent bonds are elastomeric and often require a hydrogel degradation mechanism to permit cell spreading and function.[2,3] Recently, dynamic covalent chemistry (DCC) has gained interest as an alternative cross-linking mechanism as DCC-based hydrogels have reversible linkages with tunable on−off exchange rates, enabling control over hydrogel viscoelasticity.[4,5] In particular, DCC cross-links have been used to engineer hydrogels that exhibit stress relaxation, a time-dependent matrix property that plays an important role in providing instructive and physiologically relevant cues to guide cell behavior.[6,7] In other applications, the transient nature of DCC cross-links has been leveraged to design shear-thinning and self-healing materials.[8,9] While a range of on−off exchange rates is achievable with DCC, faster relaxation time scales are often preferable to enable cell-mediated remodeling,[10] extrusion-based bioprinting,[11] and improved injectability.[12] However, rapid on−off exchange rates leads to faster hydrogel erosion,[13−16] as polymers at the edges of the hydrogel can become fully detached from the network and diffuse away, significantly limiting the use of faster-relaxing hydrogels for tissue engineering and cell culture applications.

To overcome this limitation, a common strategy is to design interpenetrating network hydrogels, with a DCC-cross-linked network intermingled with a static covalently cross-linked network.[13,14,17] For example, to stabilize fast stress-relaxing

Received: August 15, 2025
Revised: December 2, 2025
Accepted: December 3, 2025
Published: December 11, 2025

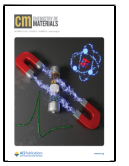

hydrogels for culture of mesenchymal stromal cells, a dual-network hydrogel cross-linked with dynamic hydrazone bonds was stabilized with a secondary SPAAC-cross-linked network.[13,14] This design resulted in long-term stability of biomimetic hydrogels for 3D cell culture; however, the networks typically have limited injectability and extrudability due to the static network. A complementary approach is through sequential cross-linking of the hydrogel, where a shear-thinning, DCC-cross-linked network is first injected or extruded, followed by secondary cross-linking via static covalent bonds to stabilize the network.[18,19] This design resulted in successful injectability; however, the final hydrogel network typically exhibits elastic behavior.[18] Other methods have incorporated secondary static cross-linking networks to stabilize highly dynamic physical gels,[20−23] but these approaches typically result in the static network having a significant impact on the viscoelastic properties. Therefore, when designing dynamic covalent hydrogels for biological applications, it is crucial to consider the trade-off between cellular-scale matrix dynamics with bulk hydrogel stability.

Here, we present an alternative biomaterials strategy to achieve single-network, viscoelastic, injectable hydrogels with long-term stability. Specifically, we hypothesized that sparse distribution of static covalent cross-links onto each polymer within a single, dynamic network would significantly improve stability without compromising injectability and viscoelasticity. Each polymer would still maintain significant conformational flexibility to dynamically rearrange its local network due to the prevalence of DCC cross-links. However, because each polymer chain is also connected to the network through selective static covalent bonding, the polymers are unable to fully detach from the network, preventing undesired erosion. We termed this network design of sparsely distributed static covalent bonds through the hydrogel network "spot-welding."

To explore this hypothesis, we demonstrate the spot-welding concept using a previously reported family of DCC hydrogels composed of hyaluronic acid (HA) and elastin-like protein (ELP), termed HELP gels.[24] These HELP gels are cross-linked by dynamic hydrazone bonds that are compatible with 3D cell culture of neural progenitor cells,[25,26] intestinal organoids,[27] hepatic organoids,[28] and pancreatic cancer organoids.[29] Previously, these DCC-cross-linked HELP gels were limited to slower on−off bond exchange kinetics to achieve stability for weeks-long culture periods. Here, to expand the viscoelastic properties of these HELP hydrogels while maintaining their long-term stability, we demonstrate the spot-welding concept with static SPAAC bonds and dynamic hydrazone bonds with faster on−off bond exchange kinetics to create "Spot-weld (SW) HELP" gels. These SW HELP gels maintain similar stress relaxation rates, resist erosion, and exhibit improved stability compared to "Dynamic HELP" gels without the SPAAC cross-links. To highlight the versatility of SW HELP gels for tissue engineering applications that require both viscoelastic mechanics and long-term gel stability, we demonstrate the successful use of our SW HELP hydrogels for 3D cardiomyocyte culture and extrusion-based 3D printing.

MATERIALS AND METHODS

ELP Expression and Purification. ELP was recombinantly expressed in bacterial cells as previously described.[30] Briefly, BL21(DE3)pLysS *Escherichia coli* (Life Technologies) were transformed with pET15b plasmids containing the ELP sequence downstream of an inducible T7 promoter. A single transformed colony was used to inoculate a starter flask containing autoclaved growth medium (terrific broth (Thermo Fisher), 0.4% glycerol (Thermo Fisher), 100 μg/mL ampicillin (Thermo Fisher)). The starter culture was incubated overnight, while shaking, for 16 h at 37 °C, after which the culture was transferred into 12 expression flasks each containing 1 L of autoclaved growth medium. At an OD_{600} of 0.8, protein expression was induced by adding 1 mM isopropyl β-D-1-thiogalactopyranoside (IPTG; Thermo Fisher) to the culture. The cultures were incubated for an additional 7 h, and then the cells were pelleted by centrifugation and lysed in TEN buffer (10 mM tris base (Thermo Fisher), 1 mM EDTA (Thermo Fisher), 100 mM NaCl (Thermo Fisher); pH 8.0) through three cycles of freezing and thawing. After the first thaw, deoxyribonuclease (Sigma-Aldrich) and phenylmethanesulfonyl fluoride (PMSF; Thermo Fisher) were added to inhibit proteolysis. ELP purification occurred through three successive thermal cycling steps. The resulting 37 kDa protein was dialyzed against Milli-Q water for 3 days, with water changes performed three times a day, after which it was lyophilized and stored at −20 °C.

Synthesis of ELP-AZD for Static HELP. ELP was functionalized with an azide group on the primary amines as previously described.[31] Briefly, ELP was dissolved at 7.5 wt % in anhydrous dimethyl sulfoxide (DMSO; Sigma-Aldrich) and then an equal volume of anhydrous *N*,*N*-dimethylformamide (DMF; Sigma-Aldrich) was added to the same flask. Separately, azido-PEG5-acid (2 equiv per ELP amine; BroadPharm) was dissolved in equal volume DMF and then hexafluorophosphate azabenzotriazole tetramethyl uronium (HATU, 1.1 equiv per azide; Sigma-Aldrich) and 4-methylmorpholine (2.5 equiv per azide; Sigma-Aldrich) were added sequentially and allowed to react for 10 min. The azide solution was then added, dropwise, to the ELP solution and left to react overnight. The reaction was precipitated in ice-cold diethyl ether (Thermo Fisher) and dried overnight under nitrogen gas. The resulting protein was dialyzed against Milli-Q water for 3 days, with water changes performed twice daily, after which it was sterile filtered, lyophilized, and stored at −20 °C.

Synthesis of ELP-HYD for Dynamic HELP. ELP was functionalized with a hydrazine group on the primary amines as previously described.[24] Briefly, ELP was dissolved at 7.5 wt % in anhydrous DMSO and then an equal volume of anhydrous DMF was added to the same flask. Separately, tri-Boc-hydrazinoacetic acid (2 equiv per ELP amine; Sigma-Aldrich) was dissolved in equal volume DMF and then HATU (2 equiv per ELP amine) and 4-methylmorpholine (5 equiv per ELP amine) were added sequentially and allowed to react for 10 min. The tri-Boc-hydrazinoacetic acid solution was then added, dropwise, to the ELP solution and left to react overnight. The reaction was precipitated in ice-cold diethyl ether and dried overnight under nitrogen gas. To deprotect, the ELP pellets were dissolved in a solution of equal parts dichloromethane (DCM; Sigma-Aldrich) and trifluoroacetic acid (TFA; Sigma-Aldrich). After dissolution, 5% (v/v) tri-isopropylsilane (Sigma-Aldrich) was added and the reaction was allowed to proceed for 4 h under continuous stirring. The reaction was precipitated in ice-cold diethyl ether and dried overnight under nitrogen gas. The resulting protein was dialyzed against Milli-Q water for 3 days, with water changes performed twice daily, after which it was sterile filtered, lyophilized, and stored at −20 °C.

Synthesis of ELP-HYD/AZD and ELP-PEG_{12}-HYD/AZD for SW HELP. ELP-HYD/AZD was synthesized by first modifying ELP with tri-Boc-hydrazinoacetic acid, deprotecting, precipitating in ice-cold diethyl ether and drying under nitrogen overnight as described above. The resulting ELP-HYD was then further functionalized with an azide group on the tyrosine residues as previously described, using 4-phenyl-3*H*-1,2,4-triazoline-3,5(4*H*)-dione (PTAD).[32] Briefly, ELP-HYD was dissolved at 1 wt % in a solution of equal parts 100 mM sodium phosphate buffer (pH 8.0), 50 mM Tris buffer, and DMF at 4 °C. Equimolar amounts of PTAD-PEG4-azide (BroadPharm) and 1,3-dibromo-5,5-dimethylhydantoin (Sigma-Aldrich) were dissolved separately in DMF and then mixed together to activate the PTAD-azide, which should cause the solution to change colors to ruby red. The activated PTAD mixture (1.3 equiv PTAD per tyrosine, Figure

https://doi.org/10.1021/acs.chemmater.5c02162
Chem. Mater. 2025, 37, 9758−9774

S3b) was then vortexed and added to the protein solution over the course of 15 min. The reaction was allowed to proceed at 4 °C for 4 h before dialyzing against 10% (v/v) DMF for 1 day and Milli-Q water for 3 days. Samples were subsequently sterile filtered, lyophilized, and stored at −20 °C.

To synthesize ELP-PEG$_{12}$-HYD/AZD, ELP was first modified with *t*-Boc-*N*-amido-PEG12-acid (BroadPharm) on the primary amines following the same HATU-mediated amidation reaction, deprotected, dialyzed, and lyophilized as described above to yield an ELP-PEG$_{12}$-NH$_2$ intermediate. The ELP-PEG$_{12}$-NH$_2$ was then functionalized with Boc-L-cysteic acid (Santa Cruz Biotechnology) following the same HATU-mediated amidation reaction, deprotected, dialyzed, and lyophilized as described above. The cysteic acid-modified ELP was then modified with tri-Boc-hydrazinoacetic as described above. Before deprotection, the resulting Boc-protected ELP-PEG$_{12}$-HYD was then further functionalized with PTAD-PEG4-azide on the tyrosine residues as described above at a ratio of PTAD to tyrosine of 5.2:4.0. The reaction was allowed to proceed at 4 °C for 4 h before dialyzing against 10% (v/v) DMF for 1 day and Milli-Q water for 3 days and lyophilized. The resulting protein was then deprotected, dialyzed, and sterile filtered as described above. Samples were subsequently lyophilized and stored at −20 °C.

Synthesis of HA-BCN for Static HELP. Sodium hyaluronate (HA, 100 kDa; Lifecore Biomedical) was functionalized with bicyclononyne groups as previously described.[31] Briefly, HA (1 wt %) and 1-hydroxybenzotriazole (HOBt, 2 equiv per HA dimer unit; Thermo Fisher) were dissolved in 100 mM MES buffer (pH 7.0). In a separate vial, endo-BCN-amine (2 equiv per HA dimer unit; Conju-Probe) and 1-ethyl-3-(3-(dimethylamino)propyl) carbodiimide hydrochloride (EDC, 2 equiv per HA dimer unit; Thermo Fisher) were sequentially dissolved in a 5:1 solution of acetonitrile (MeCN; Sigma-Aldrich) and Milli-Q water. This solution was then added slowly into the dissolved HA solution and allowed to react overnight before dialyzing against 10% (v/v) MeCN for 2 days and Milli-Q water for 3 days. The solution was subsequently sterile filtered, lyophilized, and stored at −20 °C.

Synthesis of HA-ALD for Dynamic HELP. HA (100 kDa) was functionalized with aldehyde groups as previously described.[25] Briefly, HA (1 wt %) was dissolved in MES buffer (0.2 M MES hydrate (Sigma-Aldrich), 0.15 M NaCl; pH 4.5). After the HA was fully dissolved, propargylamine (0.8 equiv per HA dimer unit; Sigma-Aldrich) was added to the reaction mixture, and the pH was adjusted to 6.0. *N*-hydroxysuccinimide (NHS, 0.8 equiv per HA dimer unit; Thermo Fisher) and EDC (0.8 equiv per HA dimer unit) were first dissolved in MES buffer and then added sequentially to the reaction mixture. The reaction was allowed to proceed overnight to form an HA-alkyne intermediate. The reaction was dialyzed against Milli-Q water for 3 days, with water changes performed twice daily, after which it was sterile filtered, lyophilized, and stored at −20 °C.

HA-alkyne was then functionalized with aldehyde groups via copper-catalyzed azide−alkyne click chemistry to achieve HA-ALD. HA-alkyne (1 wt %) was dissolved in 10× isotonic phosphate-buffered saline (PBS; 81 mM sodium phosphate dibasic, 19 mM sodium phosphate monobasic, 60 mM sodium chloride; pH 7.4) along with 1 mg/mL β-cyclodextrin (Sigma-Aldrich). The mixture was degassed under nitrogen gas for 30 min. Sodium ascorbate (Sigma-Aldrich) and copper(II) sulfate pentahydrate (Sigma-Aldrich) were dissolved in Milli-Q water and degassed under nitrogen gas before sequentially adding them to the HA-alkyne solution to reach final concentrations of 4.52 and 0.24 mM, respectively. Ald-CH2-PEG3-azide (2 equiv per alkyne group; BroadPharm) was added to the reaction mixture, and the solution was degassed for an additional 10 min. The reaction was allowed to proceed for 24 h, and then an equal volume of 50 mM EDTA (pH 7.0) was added for 1 h to chelate the copper. The reaction was dialyzed against Milli-Q water for 3 days, with water changes performed twice daily, after which it was sterile filtered, lyophilized, and stored at −20 °C.

Synthesis of HA-ALD/BCN for SW HELP. HA (100 kDa) was first functionalized with endo-BCN-amine, dialyzed, sterile filtered, and lyophilized as described above. HA-BCN was then functionalized with Ald-CH2-PEG3-azide, dialyzed, sterile filtered, and lyophilized as described above.

NMR Characterization. To quantify the efficiency and degree of modification, samples were assessed by ^{1}H nuclear magnetic resonance (NMR) spectroscopy (Varian Inova, 600 MHz) using deuterated DMSO or D_2O (Thermo Fisher) as a solvent. For ELP, the hydrazine modification efficiency was determined by comparing the integration of methyl protons of the Boc group (δ = 1.46 and 1.39, 27H) with the aromatic protons of tyrosine (δ = 7.00 and 6.62, 4H) in Boc-protected ELP. The azide modification efficiency was determined by quantifying the peaks on the PTAD (CH_2, δ = 2.56, 2H). For ELP-PEG$_{12}$-HYD/AZD we additionally observed a peak corresponding to the PEG (δ = 3.6, 2H). For HA, the bicyclononyne modification efficiency was quantified by integrating the proton signal of the methylene group adjacent to the amine group (δ = 4.1, 2H) relative to the methyl groups on *N*-acetylglucosamine of the HA backbone (δ = 1.8, 3H). The aldehyde modification efficiency was quantified by integrating the proton signal of the aldehyde group (δ = 8.1, 1H) relative to the methyl groups on *N*-acetylglucosamine of the HA backbone (δ = 1.8, 3H).

FTIR Characterization. To validate the presence of azides on the ELP backbone, Fourier transform infrared (FTIR) spectroscopy was performed using a Nicolet iS50 FT/IR Spectrometer. The presence of an azide stretch peak near 2100 cm^{-1} confirmed the incorporation of azides. Lyophilized samples (∼1 mg) were ground together with potassium bromide (∼100 mg) and pressed into pellets using the Port-A-Press KBr Pellet Die Kit. Spectra were recorded in transmission mode at room temperature (RT) in the mid-infrared range (4000−400 cm^{-1}). Acquired data were autobaselined, normalized, and smoothed through a standard moving-average algorithm in MATLAB.

Lower Critical Solution Temperature Measurements. ELP was dissolved at 1 wt % in PBS and added to a quartz cuvette with 1 mm path length. PBS was used as a blank. Absorbance readings at 300 nm were collected on a circular dichroism instrument with a temperature controller (Jasco J-815 Spectropolarimeter). The temperature was ramped up from 4 to 65 °C at a rate of 1 °C/min. The temperature was allowed to stabilize for 10 s before each measurement.

Formation of HELP Gels. Lyophilized HA and ELP were dissolved separately at 2 wt % in 10× isotonic PBS overnight at 4 °C. The ELP solution was kept on ice until use. For Static HELP, an equal volume of HA and ELP were mixed in a tube, and 10 μL of the solution were pipetted into a 4 mm diameter, 0.8 mm height silicone mold (plasma bonded to a 12 mm circular no. 2 coverglass; Electron Microscopy Sciences). The gels were then incubated on ice for 5 min, at RT for 15 min, and at 37 °C for 10 min. For Dynamic HELP and SW HELP, 5 μL of HA were pipetted into each silicone mold and kept on ice. Five μL of ELP were then pipetted directly onto the HA and mixed by swirling the pipet tip in a circular motion. The gels were then incubated at RT for 15 min and at 37 °C for 10 min. All gels had a final concentration of 1 wt % modified HA and 1 wt % modified ELP.

Hydrogel Rheological Characterization. Gels were mixed in a tube and then immediately deposited onto the stage of an ARG2 rheometer (TA Instruments) with a 20 mm, 1° cone geometry. Heavy mineral oil was used to prevent sample desiccation over the course of the measurement. Samples were allowed to cross-link at an oscillatory strain of 1% and angular frequency of 1 rad/s following each gel's respective gelation protocol (see Formation of HELP Gels). A frequency sweep was performed to measure the shear moduli of each sample at 37 °C and 1% oscillatory strain over a frequency range of 0.1 to 100 rad/s. The storage moduli at 1 rad/s were reported. The samples were then incubated at 37 °C for 5 min at an oscillatory strain of 1% and angular frequency of 1 rad/s to allow the rheometer geometry to equilibrate. Then, a stress relaxation test was performed at a constant 10% strain over a period of 24 h. The $\tau_{1/2}$ was reported as the time required for the stress to drop to half its initial value. Shear-thinning tests were performed at oscillating shear rates of 0.1

https://doi.org/10.1021/acs.chemmater.5c02162
Chem. Mater. 2025, 37, 9758−9774

and 10 s^{-1}, and self-healing tests were performed at oscillating shear strains of 0.1 and 300%.

Hydrogel Erosion Assays. To measure ELP erosion, a fluorescently labeled ELP was synthesized via the reaction of a Cy5 NHS ester (Lumiprobe) with the remaining primary amines present on the ELP. ELP was prepared at a 9:1 ratio of unlabeled ELP to Cy5-labeled ELP. HELP gels were formulated as described above, and then 1 mL of media was added to each well. At the same time each day, 200 μL of media was collected for measurement, and then a media change was performed with 1 mL of fresh media. The fluorescence signal of the Cy5-labeled ELP in the media (640 nm excitation, 670 nm emission) was measured on a plate reader. To calculate the cumulative ELP released, we summed the fluorescence measurements across all time points and normalized by the total amount of fluorescent ELP signal from a single gel. The total amount of fluorescence from a single gel was determined by first completely degrading the remaining gel at the final time point. After 14 days, the remaining gels were treated with hyaluronidase (2000 U/mL) and elastase (250 U/mL) to completely degrade the gels. To calculate the percentage of ELP remaining in the gel at each time point, the cumulative normalized fluorescence signal was subtracted from 100.

To measure HA erosion, 40 μL HELP gels were formed at the bottom of microcentrifuge tubes and 250 μL of PBS was added to each gel. The entire volume of liquid was collected and replaced with new PBS at the indicated time points and stored at −80 °C until ready for analysis. After 14 days, the remaining gels were treated with hyaluronidase (2.86 mg/mL) and elastase (5 U/mL) to completely degrade the gels. A uronic acid assay was carried out similarly as previously described.[33] Briefly, 50 μL of each sample was added to a black, clear-bottom 96-well plate. 200 μL of sulfuric acid (Sigma-Aldrich) with 25 mM sodium tetraborate (Sigma-Aldrich) were added to each well. The plate was incubated at 100 °C for 10 min and cooled at RT for 15 min. 50 μL of 0.125% (w/v) carbazole (Sigma-Aldrich) in absolute ethanol (Thermo Fisher) were then added to each well. The plate was incubated at 100 °C for 10 min and cooled at RT for 15 min. Sample absorbance at 520 nm was measured on a plate reader immediately. A standard curve was generated with unmodified HA. To calculate the cumulative HA released, we summed the absorbance measurements across all time points and normalized by the total absorbance signal from a single gel. The total absorbance from a single gel was determined by first completely degrading the remaining gel at the final time point. To calculate the percentage of HA remaining in the gel at each time point, the cumulative normalized absorbance signal was subtracted from 100.

To characterize spatial distribution of encapsulated cargo, fluorescent microspheres were mixed with the gel precursors prior to forming HELP gels in 4 mm molds as described above such that the final concentration of fluorescent microspheres was 0.1% (w/v). At the indicated time points, fluorescence images were taken on a Leica THUNDER imager with a 10× objective.

Cardiomyocyte Differentiation and Encapsulation. Human induced pluripotent stem cells (hiPSCs) were differentiated into cardiomyocytes as previously described.[34] Briefly, hiPSCs were seeded at 500,000 cells per well of a 6-well plate coated with human embryonic stem cell (hESC)-qualified Matrigel (Corning) and expanded for 3 days in mTeSR Plus media (STEMCELL Technologies) before initiating differentiation. On day 0 of differentiation, 3 mL of B26 media, consisting of RPMI 1640 (Thermo Fisher) and B27 supplement minus insulin (2%, Thermo Fisher), supplemented with 6 μM CHIR99021 (Selleck Chemicals) were added to each well. On day 2, 2 mL of B26 media were added to each well without aspirating the existing media. On day 3, the media was replaced with 3 mL of fresh B26 media supplemented with 2 μM Wnt-C59 (Selleck Chemicals). On day 5, the media was replaced with 3 mL of fresh B26 media. On day 7, the media was replaced with 3 mL of fresh B27 media, consisting of RPMI 1640 and B27 supplement with insulin (2%, Thermo Fisher). On day 9, the media was replaced with 2 mL of RPMI 1640 minus glucose (Thermo Fisher) and B27 supplement with insulin. The resulting cardiomyocytes were encapsulated at day 11.

Before encapsulation, cardiomyocytes were dissociated with TrypLE Select Enzyme 10× (Thermo Fisher), pelleted by centrifugation, and counted. Cell pellets were resuspended in 2 wt % ELP solution at 2× the desired final cell density (i.e., 1×10^5 cells/μL for a final cell density of 5×10^4 cells/μL). The cell suspensions were mixed thoroughly, and 10 μL gels were cast in 4 mm diameter, 0.8 mm height silicone molds, which were then placed into 24-well plates for culture. The gels were allowed to cross-link as described above before adding B27 media. Media was replenished every other day.

Characterization of Encapsulated Cells. To assess cell viability, hydrogels were incubated in calcein-AM (2 μM; Invitrogen) and ethidium homodimer-1 (4 μM; Invitrogen) for 10 min at 37 °C. The gels were then inverted onto a glass coverslide and imaged with a confocal microscope (Leica SPE) using a 20× air objective.

To perform immunostaining, hydrogels were fixed with 4% paraformaldehyde in PBS at RT for 20 min before washing with PBS three times for 10 min each. Samples were permeabilized with PBS-T (0.25% (v/v) Triton X-100 in PBS) for 1 h at RT and then blocked with 5% (v/v) goat serum (Gibco), 5% (w/v) bovine serum albumin (BSA; Roche), and 0.5% Triton X-100 in PBS for 3 h at RT. The following primary antibodies were diluted in antibody dilution solution (PBS with 2.5% (v/v) goat serum, 2.5% (w/v) BSA, and 0.5% (v/v) Triton X-100): mouse anti-cardiac troponin T (1:200, Invitrogen, ma5-12960) and rabbit anti-sarcomeric alpha actinin (1:200, Abcam, ab137346). The samples were incubated with the primary antibody solution for 48 h at 4 °C. After incubation, the samples were washed with PBS-T three times for 30 min each, and then the following secondary antibodies were diluted in antibody dilution solution: goat anti-rabbit Alexa Fluor 488 (1:500, Invitrogen, A-11008) and goat anti-mouse Alexa Fluor 594 (1:500, Invitrogen, A-11032). At this step, 4′,6-diamidino-2-phenylindole (DAPI; 1 μg/mL, Cell Signaling, 4083s) was also included to stain cell nuclei. The samples were incubated with the secondary antibody solution overnight at 4 °C. The following day, samples were washed with PBS-T three times for 20 min each and then mounted onto no. 1 coverslips with ProLong Gold AntiFade Mountant (Thermo Fisher). Images were acquired using a confocal microscope (Leica SPE) using either a 20× air or 63× oil objective.

Image Analysis. Sarcomeric α-actinin expression and cardiac troponin T expression were quantified using CellProfiler. Cells were immunolabeled with the relevant antibodies and identified using "IdentifyPrimaryObjects" with the "Minimum Cross-Entropy" thresholding methods, followed by "MeasureImageAreaOccupied". To quantify beating rate and contraction area, videos were recorded for 10−20 s, at 0.5 s intervals, using a brightfield image microscope. To calculate the displacement field of the beating hiPSC-CMs, individual frames of brightfield images were extracted from time-lapse videos and analyzed using PIV-MyoMonitor, an open-source particle imaging velocimetry-based software that applies a particle image velocimetry software for contractility analysis.[35] Corresponding heat map images were created, and ImageJ was used to quantify the % of highlighted pixels per frame.

3D Printing. 3D printing was carried out on a custom-built bioprinter modified from an M2 Rev E plastic 3D printer (MakerGear) as previously described.[35] Briefly, the thermoplastic extruder of the printer was removed and replaced with a mount designed to hold Replistruder 4 syringe pumps, while the control board was replaced with a Duet 2 WiFi board with RepRapFirmware.[36] Each ink material was loaded into a 2.5 mL Hamilton syringe and allowed to gel in the syringe at RT for 30 min before printing. The lattices (9 mm × 9 mm, 6 windows each) were printed on glass slides with 27 G blunt needles with an extrusion width of 0.21 mm.

The printability of each ink material was tested by assessing the shape fidelity of the printed lattices. After printing, the lattices were imaged using a Leica THUNDER microscope in brightfield mode (2.5× air objective, tile-scan). The window printability (Pr_w) and ink spreading (Sp) were quantified using eqs 1 and 2, respectively:[37,38]

https://doi.org/10.1021/acs.chemmater.5c02162
Chem. Mater. 2025, 37, 9758−9774

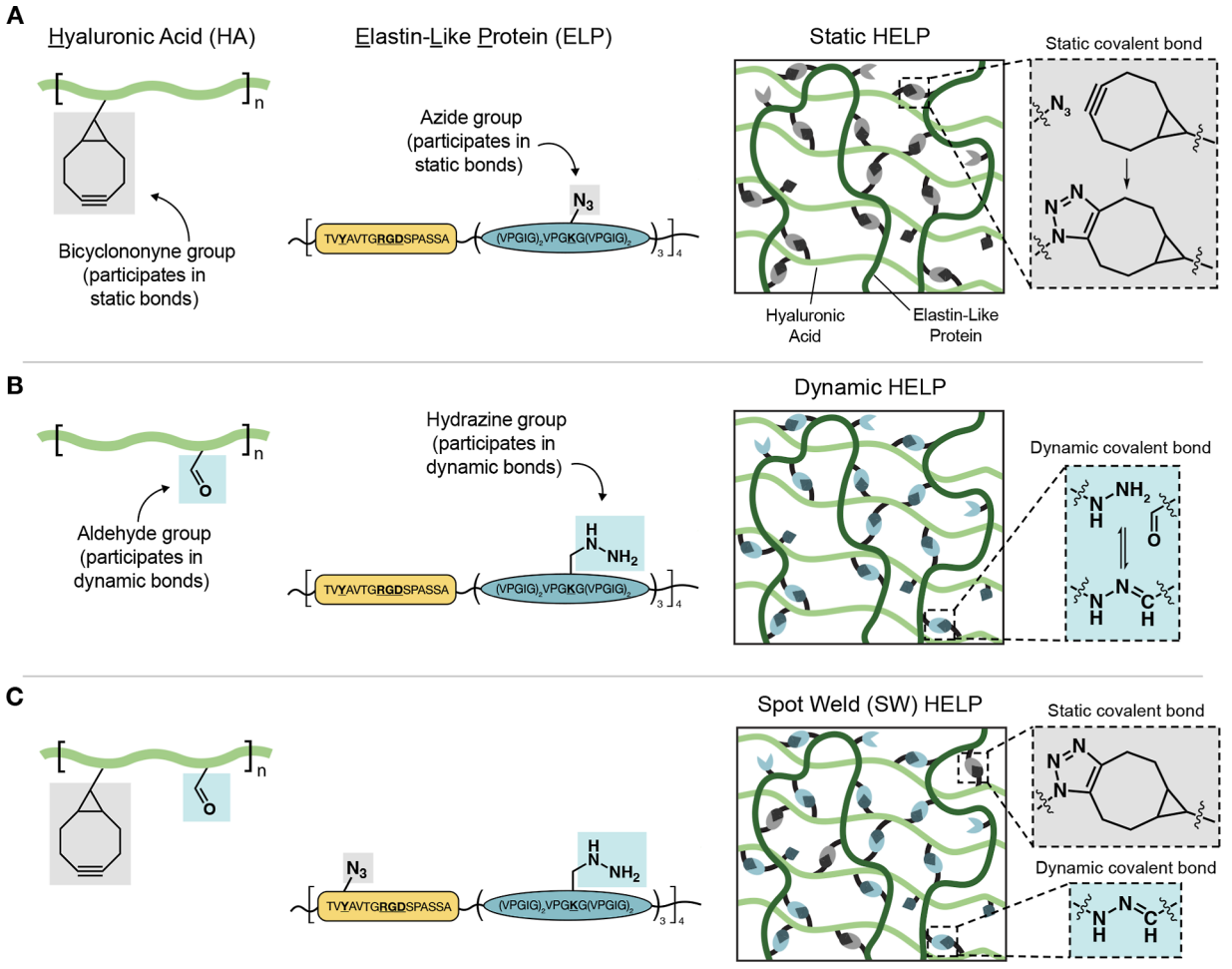

Figure 1. Approach for static, dynamic, and spot-weld cross-linking of hyaluronic acid and elastin-like protein in HELP hydrogels. (A) Schematic illustration of Static HELP hydrogels formed when static covalent cross-links occur between bicyclononyne-functionalized HA and azide-functionalized ELP. (B) Schematic illustration of Dynamic HELP hydrogels formed when dynamic covalent cross-links occur between aldehyde-functionalized HA and hydrazine-functionalized ELP. (C) Schematic illustration of Spot-weld (SW) HELP hydrogels formed from bicyclononyne- and aldehyde-functionalized HA and azide- and hydrazine-functionalized ELP.

$$\mathrm{Pr}_w = \frac{L^2}{16A_a} \tag{1}$$

$$\mathrm{Sp} = \frac{A_t - A_a}{A_t} \times 100\% \tag{2}$$

where A_a and A_t are the actual and theoretical areas of the printed window, respectively, and L is the perimeter of the window. An ink material that prints with ideal shape fidelity would have window printability $\mathrm{Pr}_w = 1$ and ink spreading $\mathrm{Sp} = 0$.

Statistical Analysis. Statistical analysis and plotting were performed using GraphPad Prism version 10 software. In vitro experiments had at least three independent gel samples in each experiment. No outlier tests were performed, and all data points were included in the analyses. All errors are reported as the standard deviation of error (SD). Details of specific statistical methods for each figure are included within the figure captions. For all studies, not significant (ns; $p > 0.05$), *$p < 0.05$, **$p < 0.01$, ***$p < 0.001$, and ****$p < 0.0001$.

RESULTS AND DISCUSSION

Designing a Single-Network Hydrogel with Both Static and Dynamic Covalent Bonds. We designed a series of single-network HELP hydrogels consisting of HA and ELP, with either static covalent bonds alone, dynamic covalent bonds alone, or both bond types (Figure 1). Here, HA was chosen as it is a key component of the ECM that provides essential biophysical and biochemical signals.[39,40] Additionally, HA possesses a high degree of chemical functionality and hydrophilicity, making it amenable to appending and solvating a variety of dynamic and static cross-linking groups.[39,41] The ELP variant used here is a previously reported engineered protein featuring elastin-like domains interspersed with integrin-binding domains derived from the ECM protein fibronectin.[32,42] This highly specific amino acid sequence enables both cellular recognition as well as site-specific bioconjugation reactions, where the degree of functionalization can be carefully controlled by the availability of specific amino acids. Together, HA and ELP serve as ideal biopolymers for engineering single-network hydrogels as they merge cellular compatibility with the ability to precisely customize the density and type of cross-linking motif.

To form HELP gels with static covalent cross-links (Static HELP), HA is modified with a bicyclononyne group to yield HA-BCN, and ELP is modified with an azide group to yield ELP-AZD (Figure 1a). When these two components are mixed, static covalent bonds are formed through a copper-free SPAAC reaction, resulting in an elastomeric hydrogel (Figure 1a).[31] To form HELP gels with DCC cross-links (Dynamic

https://doi.org/10.1021/acs.chemmater.5c02162
Chem. Mater. 2025, 37, 9758−9774

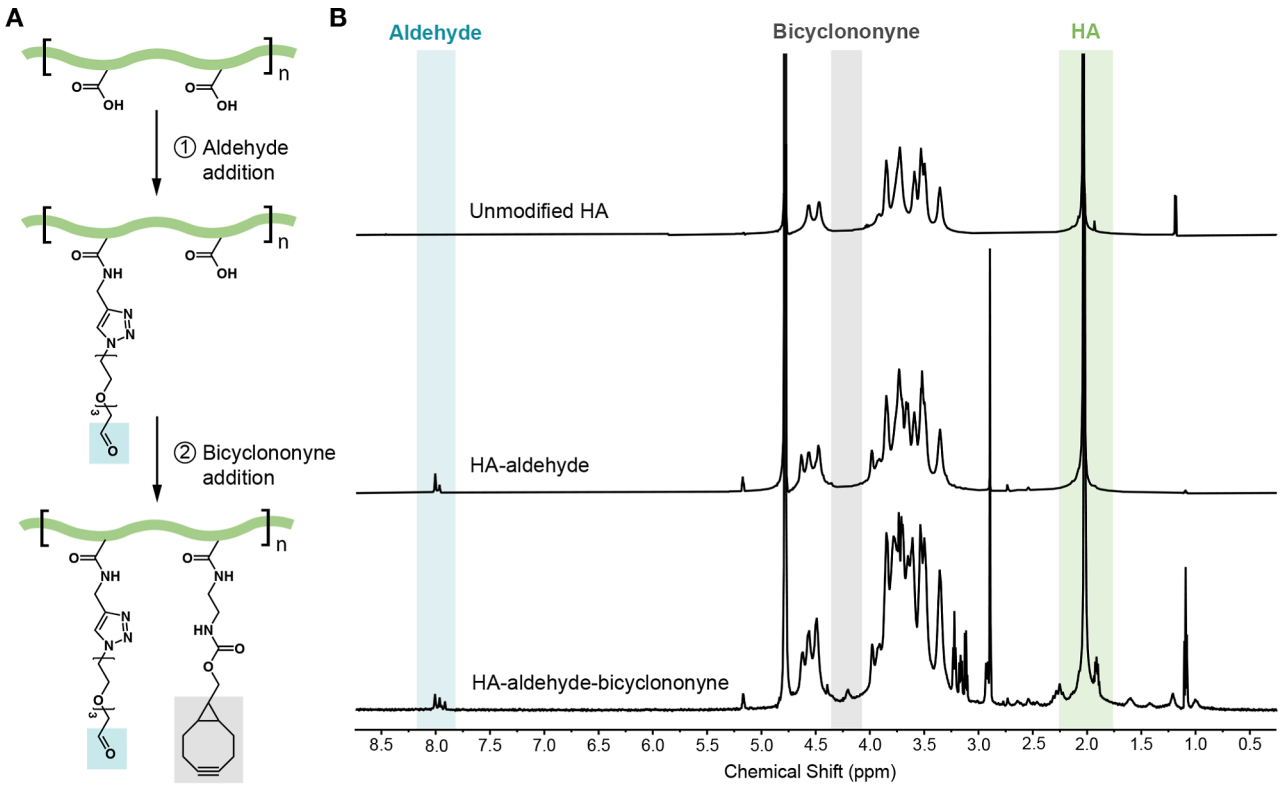

Figure 2. HA is modified with aldehyde and bicyclononyne functional groups for spot-welding. (A) Schematic illustration of sequential chemical modification steps to synthesize HA-ALD/BCN. (B) NMR spectra (600 MHz in D_2O) of unmodified HA, HA-ALD, and HA-ALD/BCN demonstrate the emergence of a peak at 7.90 ppm, corresponding to the addition of the aldehyde group, and a peak at 4.10 ppm, corresponding to the addition of the bicyclononyne group.

HELP), HA is modified with aliphatic aldehyde groups to yield HA-ALD, and ELP is modified with hydrazine groups to yield ELP-HYD (Figure 1b). Upon mixing HA-ALD and ELP-HYD, dynamic covalent hydrazone cross-links stabilize the hydrogel network while permitting matrix stress relaxation (Figure 1b).[10,25] Unfortunately, hydrogels formed through the cross-linking of aliphatic aldehydes and hydrazines are prone to rapid erosion due to the fast exchange rates of these DCC cross-links,[13,14] rendering them ill-suited for the longer time scales required for 3D cell culture and tissue engineering applications. To overcome this limitation and enhance the stability of these DCC-based HELP gels, we were inspired by a common technique used in the metals manufacturing industry, spot-welding, where small localized spots join separate sheets of metal together. To form HELP gels with spot-welds (SW HELP), we combined both static covalent SPAAC cross-links and dynamic hydrazone cross-links within a single-network hydrogel. Specifically, the HA is modified with both bicyclononyne groups and aldehyde groups to yield HA-ALD/BCN, and the ELP is modified with both azide groups and hydrazine groups to yield ELP-HYD/AZD (Figure 1c). We envisioned that this distinct combination of chemistries would enhance the mechanical integrity while preserving the viscoelastic properties of Dynamic HELP gels to enable matrix remodeling and injectability.

To synthesize HA-ALD/BCN for SW HELP, HA with a molecular weight of 100 kDa was modified through sequential reactions to enable both static and dynamic covalent cross-linking. First, HA was modified with an alkyne group via a 1-ethyl-3-(3-(dimethylamino)propyl)carbodiimide (EDC)-mediated amidation reaction between the carboxylic acid on the HA and propargylamine to form an HA-alkyne intermediate (Figure S1). Following this intermediate step, a subsequent copper-catalyzed click reaction between HA-alkyne and a heterobifunctional azide-aldehyde molecule produced HA-ALD (Figure 2a). To achieve robust hydrogel mechanical properties, we aimed for a 10−12% degree of aldehyde modification, which has previously been demonstrated to yield a Dynamic HELP hydrogel with a storage modulus of ∼800 Pa.[26] Nuclear magnetic resonance (NMR) characterization revealed the appearance of a peak at 7.90 ppm, corresponding to the protons on the triazole linkage, indicating that the HA-ALD was ∼11% modified before the introduction of the static binding ligands (Figure 2b). Following the synthesis and characterization of HA-ALD, a subsequent EDC-mediated reaction catalyzed by 1-hydroxybenzotriazole (HOBt) was carried out between the remaining available carboxylic acids on the HA-ALD biopolymer and a bicyclononyne-amine molecule (Figure 2a). The resulting HA-ALD/BCN was then characterized by NMR to verify the presence of both dynamic and static binding ligands (Figure 2b). The subsequent amidation reaction did not alter the degree of aldehyde modification (∼11%), and a similar degree of bicyclononyne modification (∼15%) was achieved.

ELP was modified with the corresponding static and dynamic reaction partners to enable the formation of a single-network hydrogel. The modularity of ELP enables precise design of amino acid sequences for site-specific bioconjugation reactions. By selecting the primary amino acid sequence, we controlled the position and frequency of reactive residues to introduce orthogonal cross-linking chemistries. Specifically, lysine (K) and tyrosine (Y) residues

https://doi.org/10.1021/acs.chemmater.5c02162
Chem. Mater. 2025, 37, 9758−9774

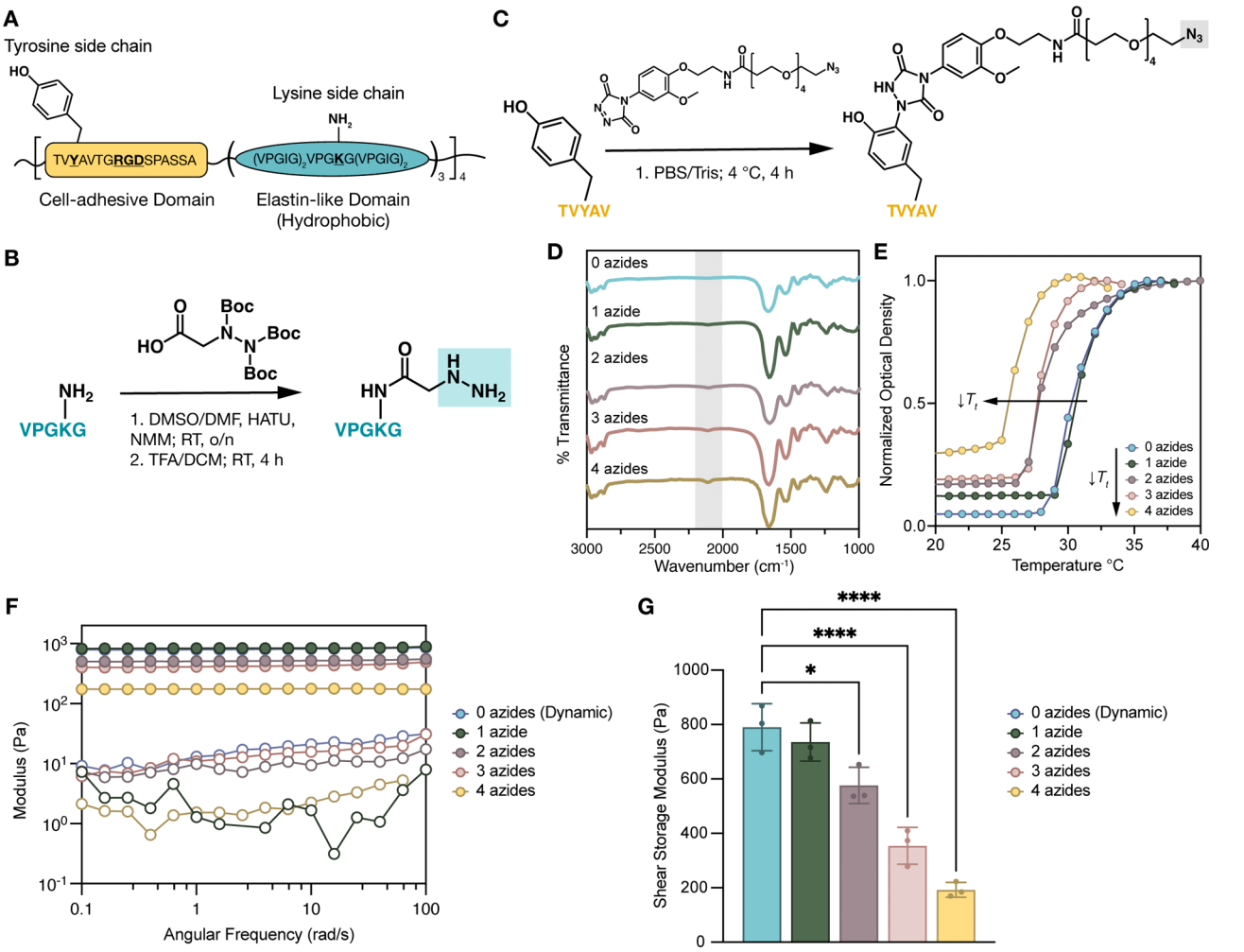

Figure 3. Azide modification of ELP alters the transition temperature (T_t) and resulting hydrogel stiffness. (A) Amino acid sequence of ELP cell-adhesive domain and elastin-like domain, which contains the lysine amino acid (K) used for coupling to hydrazine groups and the tyrosine amino acid (Y) used for coupling to azide groups. (B) Reaction conditions for the conjugation of hydrazine groups to lysines in ELP. (C) Reaction conditions for the conjugation of azide groups to tyrosines in ELP. (D) FTIR observation of azide functional group stretching (~2100 cm^{-1}) before and after coupling reactions. (E) Representative normalized optical density measurements to characterize the T_t of ELP-HYD modified with 0 azides and ELP-HYD/AZD modified with 1, 2, 3, and 4 azides (1% w/v in PBS) as a function of temperature. (F) Representative frequency sweeps performed at a fixed strain of 1% showing storage moduli (G', filled symbols) and loss moduli (G'', open symbols) for HELP gels formed with ELP-HYD modified with 0 azides and ELP-HYD/AZD modified with 1, 2, 3, and 4 azides. (G) Average shear storage moduli (G') of HELP gels formed with ELP-HYD modified with 0 azides and ELP-HYD/AZD modified with 1, 2, 3, and 4 azides (N = 3 gels, data are averages ± standard deviation). Statistical analyses performed as two-way ANOVA with Tukey's multiple comparisons test (G). *p < 0.05 and ****p < 0.0001.

(13 and 4 per ELP chain, respectively) were targeted for modification (Figure 3a). First, the primary amines on the lysine residues (along with the primary amine at the N-terminus) were modified with hydrazine functional groups via a hexafluorophosphate azabenzotriazole tetramethyl uronium (HATU)-mediated amidation reaction, yielding ELP-HYD (Figure 3b). NMR characterization revealed ~99.6% modification of the available primary amines (Figure S2). To then specifically functionalize the tyrosine residues, we conjugated azide-bearing molecules via a tyrosine-selective ene-type reaction (Figure 3c). By tuning the molar ratio of azide/tyrosine, we were able to carefully control the number of azide functional groups per ELP from 1 to 4, as characterized by NMR (Figure S3). Additionally, Fourier transform infrared (FTIR) spectroscopy revealed the appearance of an azide stretch at ~2100 cm^{-1} (Figure 3d), confirming the successful modification of ELP-HYD/AZD with 1, 2, 3, and 4 azides per ELP.

ELPs display lower critical solution temperature (LCST) behavior, where above a characteristic transition temperature, T_t, the protein polymer undergoes an entropically driven phase separation.[43,44] Our previous work has demonstrated the tunability of the T_t through altering protein hydrophilicity.[31] Because the azide-bearing groups are highly hydrophobic, we hypothesized that the addition of increasing numbers of azides may decrease the T_t. This change in T_t would result in the formation of protein-rich aggregates that could impact hydrogel mechanical properties,[31] so we sought to characterize the T_t of the newly modified ELP polymers. As expected, optical density measurements revealed a trend of decreasing T_t as the number of azides per ELP increased (Figure 3e). Additionally, when cross-linked with HA-ALD/BCN, all ELP variants formed hydrogels (Figure 3f), but the resulting HELP

https://doi.org/10.1021/acs.chemmater.5c02162
Chem. Mater. 2025, 37, 9758−9774

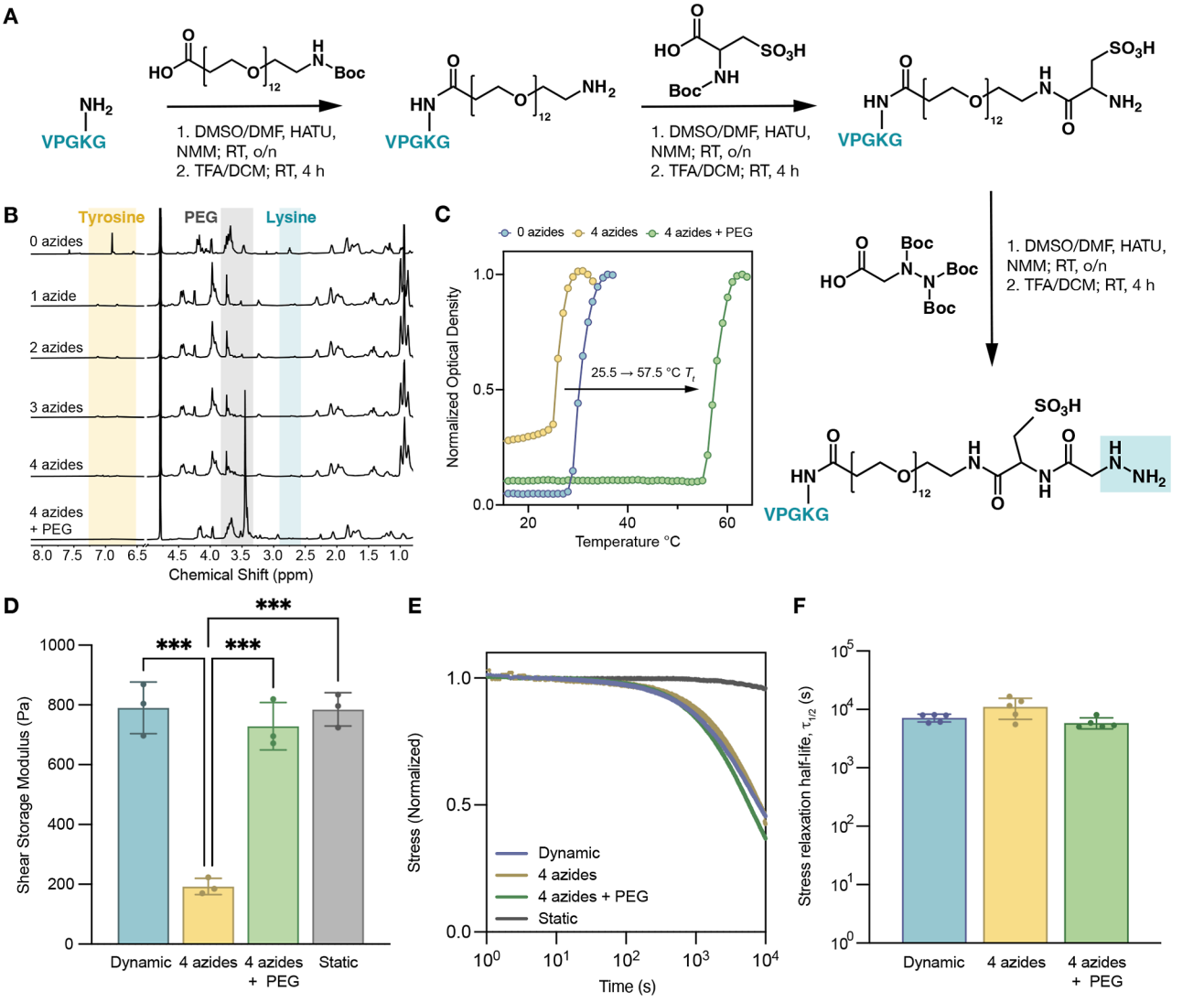

Figure 4. Engineering a SW HELP gel with similar viscoelastic properties to Dynamic HELP. (A) Reaction conditions and intermediates for the synthesis of ELP-PEG_{12}-HYD, containing a hydrophilic 12-mer PEG and cysteic acid linker. The primary amine of the ELP lysine residue is first modified with a Boc-protected PEG_{12}-amine, followed by a Boc-protected cysteic acid, and finally with a hydrazine functional group. (B) NMR spectra (600 MHz in D_2O) of ELP before and after functionalization demonstrate a decreased peak at 2.75 ppm attributed to reaction of the primary amine side chain on lysine residues. (C) Representative normalized optical density measurements of ELP-HYD modified with 0 azides, ELP-HYD/AZD modified with 4 azides, and ELP-PEG_{12}-HYD/AZD modified with 4 azides (1% w/v in PBS) as a function of temperature. (D) Average shear storage moduli (G') of HELP gels formed with only dynamic covalent cross-links (termed Dynamic), a combination of dynamic and static cross-links using ELP-HYD/AZD with 4 azides (termed 4 azides), a combination of dynamic and static cross-links using the hydrophilic ELP-PEG_{12}-HYD/AZD with 4 azides (termed 4 azides + PEG), and static covalent cross-links only (termed Static) (N = 3 gels, data are averages ± standard deviation). (E,F) Normalized representative stress relaxation curves (E) and stress relaxation half-lives ($\tau_{1/2}$, F) of HELP gel formulations shown in panel (D). (N = 5 gels, data are averages ± standard deviation). Statistical analyses performed as two-way ANOVA with Tukey's multiple comparisons test (D,F). ***$p < 0.001$.

gels exhibited a concomitant decrease in storage modulus as the number of azides per ELP increased (Figure 3g). With the addition of 4 azides, the resulting storage modulus was ~200 Pa, significantly decreased from Dynamic HELP gels with no azides (~800 Pa). This decrease in storage modulus has been previously attributed to the assembly of ELP aggregates above the T_t that obscure available cross-linking sites on the ELP.[31] Taken together, these results indicate that conjugation of ELP with an increasing number of azide moieties lowers the T_t, which in turn decreases the storage modulus of the resulting HELP hydrogel.

Tuning ELP Hydrophilicity Yields Stiffness-Matched SW HELP Gels. To incorporate SPAAC cross-links into the HELP hydrogels while maintaining constant hydrogel stiffness, we devised an alternative bioconjugation strategy for hydrazine functionalization. In our previous work, we demonstrated that protein hydrophilicity could be tuned by conjugating the ELP with increasingly hydrophilic molecules, which in turn modulates the resulting protein solubility and T_t.[31] Therefore, we hypothesized that bioconjugation of a more hydrophilic, hydrazine-containing molecule would offset the decrease in hydrophilicity due to the conjugation of hydrophobic azide groups.

To increase the hydrophilicity of the hydrazine functional group, a 12-mer polyethylene glycol (PEG) and cysteic acid linker were first conjugated to the primary amines of ELP via

https://doi.org/10.1021/acs.chemmater.5c02162
Chem. Mater. 2025, 37, 9758−9774

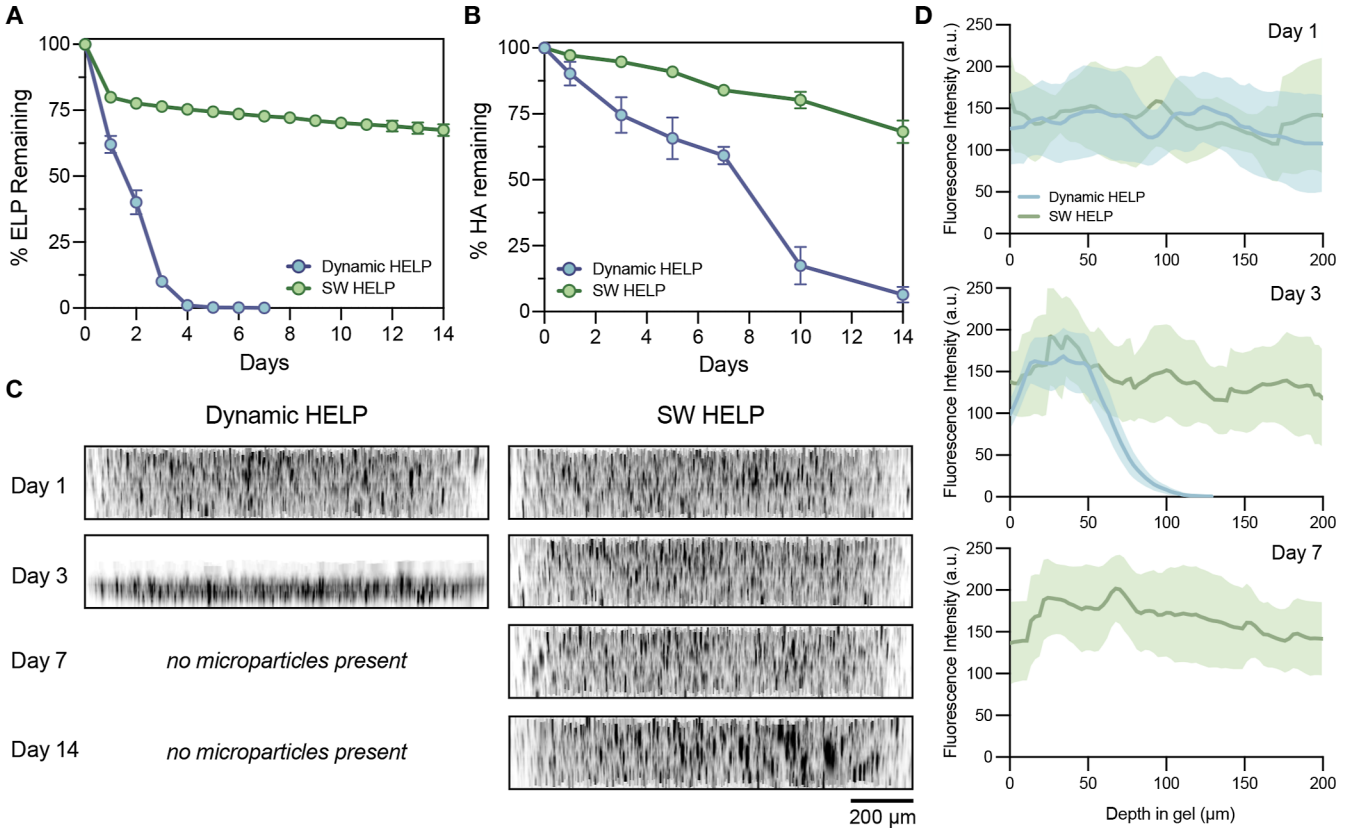

Figure 5. SW HELP gels with sparse static cross-links exhibit enhanced stability compared to Dynamic HELP gels. (A) Quantification of Cy5-labeled ELP remaining in Dynamic HELP and SW HELP gels over 14 days of exposure to media ($N = 4$ gels, data are means ± standard deviation). (B) Quantification of HA remaining in Dynamic HELP and SW HELP gels over 14 days of exposure to phosphate buffered saline (PBS) ($N = 4$ gels, data are means ± standard deviation). (C) Representative fluorescence reconstructions showing $y-z$ planes of fluorescent microparticles encapsulated within Dynamic HELP and SW HELP gels over 14 days of exposure to media. (D) Measurement of fluorescence intensity across gel depth (z-direction, where $z = 0$ is the bottom of the gel) of fluorescent microparticles encapsulated within Dynamic HELP and SW HELP gels at days 1, 3, and 7 ($N = 5$ gels, shaded bands represent 95% confidence intervals of the respective means).

the same HATU-mediated amidation reaction before the addition of the hydrazine functional group, yielding ELP-PEG_{12}-HYD (Figure 4a). PEG molecules have been used in a variety of systems to increase polymer solubility and have been demonstrated to be cell compatible.[45−47] Cysteic acid is a modified version of the naturally occurring amino acid cysteine with a highly hydrophilic sulfonic acid group that has also been used to increase the solubility of various molecules.[48,49] Thus, the combination of the two hydrophilic moieties was expected to substantially increase ELP hydrophilicity. Following hydrazine addition, the azide groups were then conjugated to the tyrosine residues on the ELP following the same protocol as before, yielding ELP-PEG_{12}-HYD/AZD.

We chose to incorporate the hydrophilic linker to the ELP containing 4 azides as this would provide the maximum amount of static SPAAC cross-links possible within the current system, resulting in a ratio of 4 azide groups to 14 hydrazine groups per ELP chain. Using the Flory−Stockmayer gelation model, we predicted the percolation threshold, p_c, of a hydrogel with 4 azide groups per ELP chain and 37.5 bicyclononyne groups per HA chain to be 0.178.[50] This means that only 17.8% of the SPAAC cross-links within the hydrogel must be reacted to form a percolating network of static bonds. In contrast, a system with only 2 azide groups per ELP chain has a theoretical p_c of 0.436, which implies a much higher SPAAC cross-linking efficiency would need to be achieved to form a percolating network of static bonds. NMR characterization revealed the disappearance of a peak at 2.75 ppm, which is assigned to the lysine residue,[51] confirming that the lysine-targeting reactions were successful (Figure 4b). Additionally, the increased peak at 3.50 ppm, corresponding to PEG, confirmed the successful modification of ELP-PEG_{12}-HYD (Figure 4b). As expected, the addition of the hydrophilic PEG and cysteic acid linker was sufficient to shift the T_t from ∼25.5 °C for ELP-HYD/AZD with 4 azides to ∼57.5 °C for ELP-PEG_{12}-HYD/AZD with 4 azides (Figure 4c).

As this new T_t is substantially higher than temperatures used in mammalian cell culture protocols, we anticipated that this ELP with the hydrophilic PEG and cysteic acid linker would ameliorate the previously observed aggregation-induced decrease in hydrogel stiffness. To confirm this, we cross-linked ELP-HYD, ELP-HYD/AZD with 4 azides, and ELP-PEG_{12}-HYD/AZD with 4 azides (each at 1 wt %) with the same dual-functionalized HA-ALD/BCN (1 wt %) as before (Figure 2a). When ELP-PEG_{12}-HYD/AZD was mixed with HA-ALD/BCN (denoted as "4 azides + PEG"), the stiffness was significantly increased compared to ELP-HYD/AZD (denoted as "4 azides"), yielding a shear storage modulus of ∼730 Pa (Figure 4d). Importantly, the shear storage modulus of the hydrogel formed with ELP-PEG_{12}-HYD/AZD was not significantly different from that of Dynamic HELP gels formed with ELP-HYD (containing 0 azides) (Figures 4d and S4a,b). Therefore, increasing the T_t through altering protein hydrophilicity was

https://doi.org/10.1021/acs.chemmater.5c02162
Chem. Mater. 2025, 37, 9758−9774

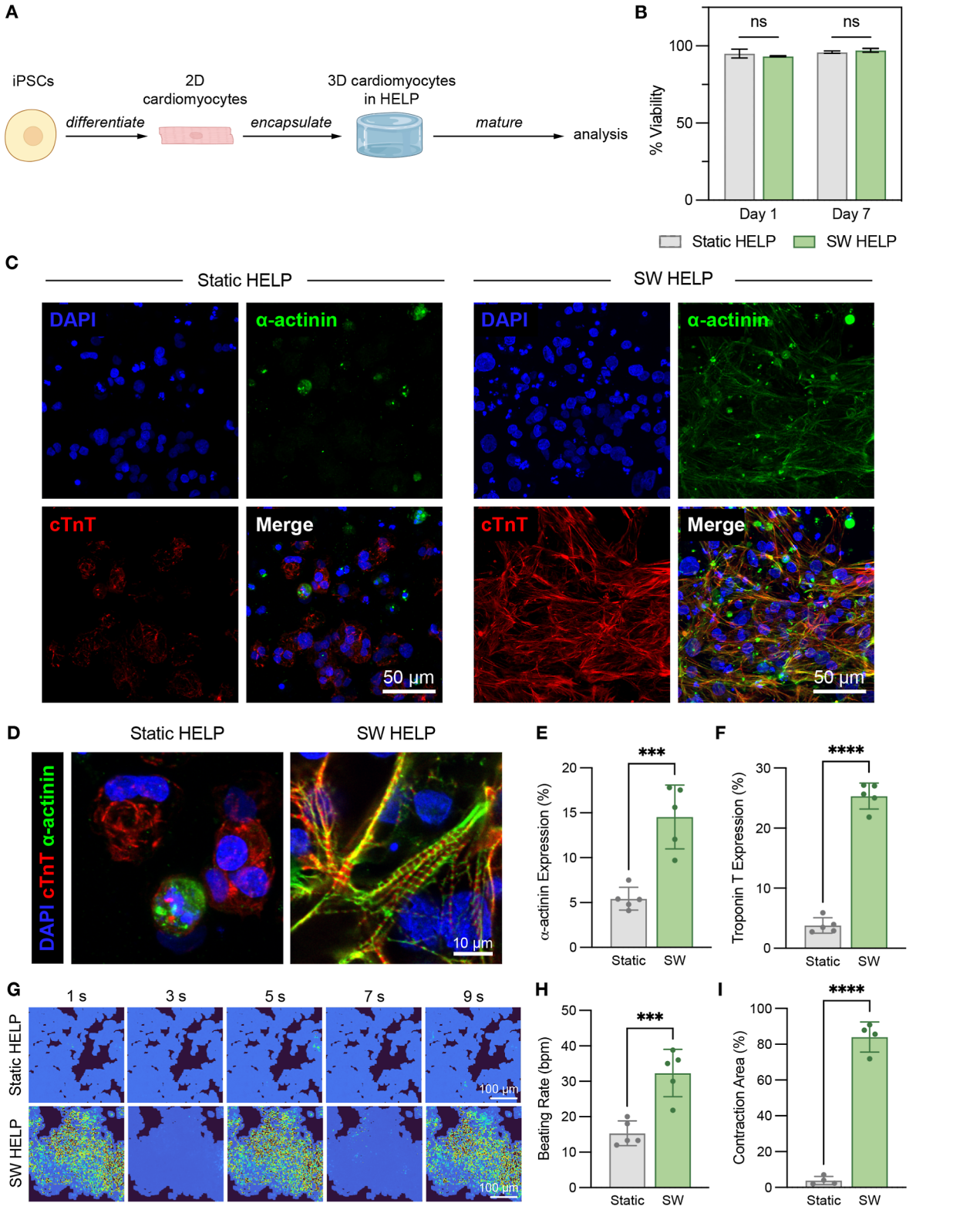

Figure 6. SW HELP gels support the 3D culture of hiPSC-CMs. (A) Schematic of experimental workflow for cardiomyocyte differentiation and encapsulation experiments. (B) Quantification of cell viability after 1 and 7 days of culture (N = 3 gels, data are means ± standard deviation). (C) Representative maximum projection fluorescence images of hiPSC-CMs encapsulated within Static HELP and SW HELP gels after 14 days labeled for cardiac troponin T (cTnT, red) and α-actinin (green). Nuclei are counterstained with DAPI (blue). (D) Higher-magnification representative maximum projection fluorescence images of hiPSC-CMs encapsulated within Static HELP and SW HELP gels after 14 days. (E,F) Quantification of the percentage of α-actinin expression (E) and cardiac troponin T expression (F) in Static HELP and SW HELP gels after 14 days (N = 5 gels, data are means ± standard deviation). (G) Displacement vector field heat maps generated from hydrogel contraction videos of hiPSC-CMs encapsulated within Static HELP and SW HELP gels after 14 days. Blue and black backgrounds designate areas where the tracking algorithm could and could not identify fiducial markers, respectively. (H,I) Quantification of beating rate (H) and contractile area (I) of hiPSC-CM cultures within

https://doi.org/10.1021/acs.chemmater.5c02162
Chem. Mater. 2025, 37, 9758−9774

Figure 6. continued

Static HELP and SW HELP gels after 14 days (N = 5 gels, data are means ± standard deviation). Statistical analyses performed as two-way ANOVA with Šidák's multiple comparisons test (B) and two-tailed unpaired t-test (E,F,H,I). ***p < 0.001 and ****p < 0.0001.

able to increase hydrogel stiffness, consistent with the idea that the cross-linking groups were being obscured at a lower T_t.

The viscoelastic properties of the HELP gels were next evaluated through a stress relaxation test, where a constant 10% strain was applied, and the resulting stress was measured over time (Figure 4e). A 10% strain falls within the linear viscoelastic regime of the HELP gels (Figure S4d−f). Interestingly, the addition of the 4 azides in either ELP-HYD/AZD ("4 azides") or ELP-PEG$_{12}$-HYD/AZD ("4 azides + PEG") did not significantly affect the stress relaxation profile or half-life ($\tau_{1/2}$), with all three stress-relaxing conditions resulting in a $\tau_{1/2}$ of ∼6000 s (Figure 4e,f). This suggests that the presence of sparsely distributed static covalent bonds has a negligible effect on gel relaxation. Taken together, we have demonstrated a method to functionalize ELP with azide groups that can participate in sparse static covalent cross-linking while maintaining the stiffness and stress relaxation rate of Dynamic HELP gels. Given the similar shear storage moduli and stress-relaxing properties to the Dynamic HELP gels, subsequent studies were carried out with HELP hydrogels formed using ELP-PEG$_{12}$-HYD/AZD containing 4 azides, henceforth referred to as SW HELP.

A static, elastic HELP gel (Static HELP) was also fabricated as a control through SPAAC-mediated covalent cross-linking between an azide-functionalized ELP (1 wt %) and a bicyclononyne-functionalized HA (1 wt %) (Figure 1a), as previously described.[31] Static HELP gels were formulated to exhibit similar stiffness to Dynamic and SW HELP gels (Figures 4d and S4c) but display minimal relaxation of stress under a constant applied strain (Figure 4e).

Sparse Static Cross-Links Improve the Stability of Viscoelastic HELP Gels. Stress-relaxing hydrogels formed through dynamic covalent bonds are prone to rapid erosion due to the fast exchange kinetics of the dynamic hydrogel cross-links.[13,14] As a result, this rapid degradation limits their potential use for both in vivo and in vitro biological applications where long-term stability or long-term culture is required. We hypothesized that incorporating static SPAAC cross-links into our dynamic hydrogel network would limit hydrogel erosion and improve long-term stability. Because the highly stable SPAAC-participating groups are directly functionalized to the polymer backbones, they serve as "spot-welds" to anchor the polymers in place and stabilize the single network hydrogel while still enabling local polymer movement to maintain viscoelastic properties.

To assess the effect of SPAAC cross-links on the stability of the hydrogel over extended time periods, HELP hydrogels were created with the following conditions: Dynamic HELP (1 wt % ELP-HYD and 1 wt % HA-ALD) and SW HELP (1 wt % ELP-PEG$_{12}$-HYD/AZD and 1 wt % HA-ALD/BCN). Polymer release from the hydrogel was then monitored over time with regular washes to simulate media changes. For ELP erosion, a fluorescently labeled ELP was incorporated in both gel formulations, and fluorescence in the media was measured over time. While the Dynamic HELP gels exhibited full loss of ELP after 4 days, the SW HELP gels dramatically limited the extent of ELP erosion, with >60% ELP remaining after 14 days (Figure 5a). For HA erosion, a colorimetric uronic acid assay was used to measure the cumulative HA released from the hydrogels over time. With the addition of SPAAC cross-links, the amount of HA remaining after 14 days increased to ∼70%, compared to only ∼6% of HA remaining for the Dynamic HELP gels without SPAAC cross-links (Figure 5b). These results indicate that incorporating a controlled amount of sparsely distributed SPAAC cross-links in a hydrogel network with dynamic covalent cross-links can tune the erosion profile of the hydrogels from days to weeks.

As an additional practical metric for characterizing hydrogel stability, we investigated the ability of the gels to retain cargo (e.g., cells or microparticles) over extended time. We loaded fluorescent microparticles into both hydrogel formulations and imaged them to determine their spatial distribution over 2 weeks. Within the Dynamic HELP gels, all the microparticles settled to the bottom of the culture plate by Day 3 and were subsequently washed away with the next media change (Figure 5c,d). The microparticles within the SW HELP gels not only remained suspended within the hydrogels over the two week period, but they also maintained a homogeneous distribution throughout the entire hydrogel (Figure 5c,d). Overall, SW HELP exhibits improved hydrogel stability and distribution of embedded cargo compared to Dynamic HELP while maintaining similar stress-relaxing properties.

SW HELP Gels Promote Cardiomyocyte Spreading and Synchronous Beating. As a demonstration of the utility of this hydrogel platform for 3D cell culture, we evaluated whether SW HELP hydrogels could support the culture of human induced pluripotent stem cell-derived cardiomyocytes (hiPSC-CMs). hiPSC-CMs are sensitive to cell−cell and cell−ECM interactions, which are known to regulate their proliferation, differentiation, and maturation.[52,53] At the same time, hiPSC-CMs require long maturation periods (∼14 days) to electrically couple and synchronize, and they also exert substantial mechanical forces on their environment as they contract.[54,55] However, in 3D matrices that exhibit long-term stability, mechanical confinement often precludes the ability of cells to undergo morphological changes and establish the cellular interconnectivity that is required for signal propagation and maturation.[6,56] Viscoelastic matrices offer a promising approach to enable cell-mediated remodeling of the matrix and overcome 3D mechanical confinement. Therefore, the 3D culture of hiPSC-CMs requires a remodelable, viscoelastic hydrogel that can withstand contractile forces over long culture periods.

We first investigated how hiPSC-CM morphology and cell fate were influenced by matrix viscoelasticity. hiPSC-CMs were differentiated in 2D following previously established protocols, and spontaneous contraction was observed on day 8−9 of differentiation. On day 12 of differentiation, spontaneously beating hiPSC-CMs were encapsulated in SW HELP gels (viscoelastic, remodelable) and Static HELP gels (more elastic, nonremodelable) and cultured for 14 days (Figure 6a). Using a live/dead cytotoxicity assay, short-term viability (24 h post-encapsulation) was ∼93% in SW HELP gels and ∼95% in Static HELP gels, indicating high cytocompatibility of the hydrogel encapsulation process (Figures 6b and S5). High cell viability was also maintained after 7 days of culture, with ∼97%

https://doi.org/10.1021/acs.chemmater.5c02162
Chem. Mater. 2025, 37, 9758−9774

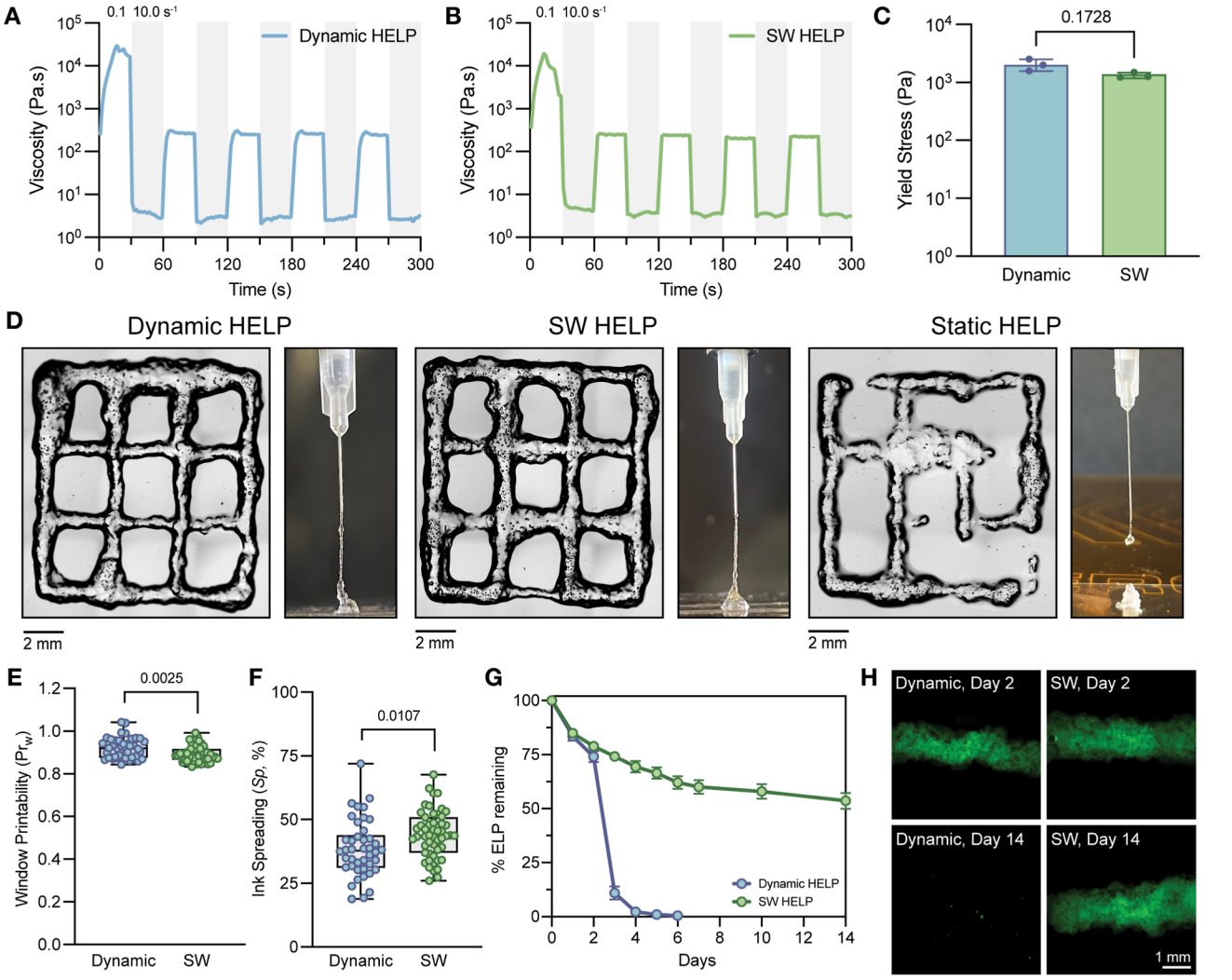

Figure 7. Printability of SW HELP gels (A,B). Viscosity recovery at high (10.0 s^{-1}) and low (0.1 s^{-1}) shear rates of Dynamic HELP (A) and SW HELP (B) gels. (C) Yield stress measurements of Dynamic HELP and SW HELP gels (N = 3 gels, data are means ± standard deviation). (D) Representative brightfield images of printed lattices (left) and photographs of ink filaments extruded from 27 G blunt needles (right) of Dynamic HELP, SW HELP, and Static HELP gels. (E,F) Quantification of window printability (Pr_w, E) and ink spreading (Sp, F) of lattices printed with Dynamic HELP and SW HELP gel inks. Data in (E,F) are plotted as box and whisker plots, with whiskers showing the minimum and maximum values, and a superimposed scatter plot where individual points represent the values for individual windows (for Dynamic, n = 42 windows from N = 5 prints; for SW, n = 51 windows from N = 6 prints). (G) Quantification of Cy5-labeled ELP remaining in Dynamic HELP and SW HELP gels over 14 days after extrusion through a 27 G blunt needle (N = 3 gels, data are means ± standard deviation). (H) Representative fluorescence images of Cy5-labeled Dynamic HELP and SW HELP gels after extrusion through a 27 G blunt needle on days 2 and 14. Statistical analyses performed as two-tailed unpaired t-test (C,E,F).

viability in SW HELP gels and ∼96% viability in Static HELP gels (Figures 6b and S5). After 14 days of culture, hiPSC-CMs were fixed and stained for the cardiomyocyte-specific protein troponin T (cTnT) and the contractile machinery protein (sarcomeric α-actinin) (Figure 6c,d). In Static HELP gels, hiPSC-CMs exhibited limited α-actinin expression and a disorganized sarcomeric structure, likely due to an inability to remodel their surrounding matrix (Figure 6d,e). In contrast, SW HELP gels supported cell-mediated remodeling of the dynamic hydrogel environment, resulting in hiPSC-CMs with a more spread morphology, increased expression of α-actinin, and maintenance of striated sarcomeres (Figure 6d,e). The ability to remodel the viscoelastic matrix also enabled the formation of an interconnected network of hiPSC-CMs within SW HELP gels, while those in Static HELP gels remained in isolated clusters. Additionally, while both conditions supported cell viability, SW HELP gels supported maintenance of the cardiomyocyte phenotype, as hiPSC-CMs in SW HELP gels exhibited significantly higher expression of cTnT compared to those in Static HELP gels (Figure 6f).

To compare cardiomyocyte functional activity in SW HELP vs Static HELP gels, we measured the global contraction behavior of the hiPSC-CM-laden hydrogels after 14 days of culture and maturation. An image analysis tool was used for automated contractility assessment of 3D cardiac tissues.[35] From this algorithm, heat maps of displacement vector fields were generated that correspond to hydrogel contraction and relaxation behavior (Figure 6g). Notably, hiPSC-CMs encapsulated within SW HELP gels displayed enhanced coordination, with large areas of the hydrogel beating synchronously (Video S1). In comparison, hiPSC-CM beating only occurred in a few sparse clusters of cells in various

https://doi.org/10.1021/acs.chemmater.5c02162
Chem. Mater. 2025, 37, 9758−9774

discrete locations throughout the Static HELP gels (Video S2), and these cells exhibited a slower beating rate (Figure 6h). The lack of synchronicity within Static HELP gels could be attributed to the poor establishment of interconnected networks in static, confining environments, which hinders the cell−cell communication required to ensure proper propagation of electrical potential. As a result, the fraction of the overall hydrogel that underwent contraction was significantly reduced in the Static HELP gels compared to the SW HELP gels (Figure 6i). Importantly, the SW HELP gels persisted in culture for 14 days despite the mechanical contractions induced by the beating cardiomyocytes, which was not observable with Dynamic HELP gels, as these fully eroded after only 4 days. These results suggest that our SW HELP platform exhibits both desirable viscoelastic properties for enabling cell−cell contact and signal propagation while also maintaining structural stability, ultimately supporting the phenotypic maintenance and synchronized contractile activity of hiPSC-CMs.

While the primary difference between SW HELP and Static HELP gels is their stress relaxation rate, they also exhibit other differences that could contribute to the observed cardiomyocyte phenotypes. Of note, the functional groups participating in cross-linking differ between the two gel conditions (primarily hydrazone in SW HELP vs primarily SPAAC in Static HELP). While SPAAC is a bioorthogonal reaction, the aldehyde groups present in SW HELP could engage with primary amines on cell surface proteins to form Schiff bases, and the potential cellular effect could be explored in future work. Additionally, the T_t of ELP-AZD used in Static HELP is ∼30 °C,[31] while the T_t of ELP-PEG$_{12}$-HYD/AZD used in SW HELP is ∼57.5 °C. This difference in the T_t could result in changes in ELP microstructure, as ELPs with a lower T_t have been reported to form ELP-rich aggregates within the hydrogel.[31] Altogether, the collective matrix properties of the SW HELP gels provide a permissive environment for hiPSC-CM culture and signal propagation, and the contributions from these individual matrix properties should be further explored in future studies.

SW HELP Gels Maintain the Injectability and Printability of Dynamic HELP Gels. In addition to 3D cell culture, another potential application that has leveraged dynamic hydrogels is 3D extrusion bioprinting. In these applications, the transient DCC cross-links provide increased injectability through a syringe that, once extruded, reform to reinforce the printed structure.[57] In our previous work, we showed that although the Dynamic HELP gel formulation was highly printable, the resulting hydrogels lacked stability and eroded over time,[11] similar to what we observed here (Figure 5). A DCC-cross-linked hydrogel with slower exchange dynamics offered enhanced hydrogel stability, but suffered in terms of printability and exhibited significantly slower stress relaxation rates.[11] In contrast, our SW HELP gels are able to maintain faster stress relaxation rates similar to Dynamic HELP gels while still maintaining hydrogel stability due to the sparsely distributed static cross-links. We hypothesized that this combination of viscoelasticity and stability would make this material an ideal bioink candidate for 3D extrusion printing.

To assess the potential for 3D printing, we first characterized the flow properties of SW HELP gels compared to Dynamic HELP gels. Both Dynamic and SW HELP gels displayed viscous shear-thinning and self-healing behavior, which is characterized by measuring the viscosity in response to alternating high (10.0 s^{-1}) and low (0.1 s^{-1}) shear rates (Figures 7a,b and S6a) and the modulus recovery in response to alternating high (300%) and low (0.1%) strains (Figure S6b,c). Additionally, upon looking closer at the transition between high and low shear rates, we observed that both hydrogel conditions quickly reached a plateau viscosity (Figure S6a), suggesting rapid self-healing behavior. We next evaluated the yield stress of the hydrogels by performing a steady state stress sweep, in which the stress is incrementally increased logarithmically.[58] The yield stress is then defined as the lowest applied stress that causes the material to yield and flow, indicated by a sharp drop in viscosity.[59] Both Dynamic and SW HELP gels were observed to have a yield stress of similar magnitude (σ_y ∼ 1−2 kPa) (Figure 7c). These data suggest that SW HELP gels should be printable despite the inclusion of sparse static cross-links.

To directly test this idea, we evaluated whether the static cross-links influenced the printability of the HELP gels during extrusion printing. Before printing, we first allowed the hydrogel network to form a fully cross-linked network within the print syringe. After this equilibration time, we printed the HELP gels into a 9 mm by 9 mm lattice structure. For both Dynamic and SW HELP gels, a continuous filament could be extruded through the print syringe, resulting in fully formed lattices (Figure 7d). In contrast, extrusion of Static HELP gels yielded broken filaments that deposited inconsistently, resulting in incomplete lattice structures (Figure 7d). Shape fidelity was quantitatively assessed from the printed lattice structures using two metrics, window printability (Pr_w) and ink spreading (Sp, also termed diffusion rate in some manuscripts[37,60]). Similar Pr_w and Sp were observed for Dynamic and SW inks, though Dynamic HELP had slightly better print fidelity (higher Pr_w and lower Sp) than SW HELP (Figure 7e,f). Despite this, Pr_w was ∼0.9 in both cases, which falls within the range (Pr_w ∼ 0.9−1.1) that has been previously demonstrated to have the best filament morphology and mechanical stability of 3D printed hydrogel constructs.[38] Furthermore, Sp ∼ 40% in both cases, which represents an improvement from other works that have optimized hydrogel ink formulations for print fidelity (Sp ∼ 60%).[61] Finally, the extruded SW HELP gels persist for at least 14 days, while the extruded Dynamic HELP gels erode completely by day 4 (Figures 7g,h and S7). Altogether, these results demonstrate that the addition of sparse static cross-links in SW HELP gels do not greatly impact printability in this system, highlighting the potential for SW HELP gels to be leveraged in 3D extrusion bioprinting applications.

■ CONCLUSION

Spot-welding of engineered hydrogels has the ability to expand the versatility of dynamic covalent hydrogels for many applications in biomaterials and tissue engineering. Here, we developed a viscoelastic, shear-thinning hydrogel where fast-exchanging DCC cross-links were stabilized by a sparsely distributed network of static SPAAC cross-links. Through targeting the unique side chains of specific amino acids on ELP, we were able to demonstrate precise control over bioconjugation of different functional groups on a single polymer. To mitigate the decrease in storage modulus that accompanied the addition of azide groups to the ELP, we altered the protein hydrophilicity to tune the T_t and reduce protein aggregation, which allowed us to generate stiffness-

https://doi.org/10.1021/acs.chemmater.5c02162
Chem. Mater. 2025, 37, 9758−9774

matched Static, Dynamic, and SW HELP gels. SW HELP gels exhibited drastically improved hydrogel stability compared to Dynamic HELP gels while maintaining statistically similar fast stress relaxation rates. Because SW HELP gels were able to withstand hydrogel erosion for at least 14 days, they were well-suited for the 3D culture of human pluripotent stem cell-derived cardiomyocytes, a highly contractile and mechanically active cell type. Using the SW HELP gel platform, we demonstrated the importance of a fast-relaxing yet long-term stable 3D hydrogel for promoting the phenotypic maintenance and synchronous contraction of cardiomyocytes. While Dynamic HELP gels may also enable sufficient matrix remodeling, their rapid erosion rates preclude the possibility of longer culture periods required for observing cardiomyocyte maturation and engineering cardiac tissues. Furthermore, the presence of SPAAC cross-links within the SW HELP gels does not impinge upon their extrudability through a print syringe, positioning SW HELP gels as ideal bioink materials for 3D bioprinting applications.

Here, we demonstrate two important biological applications that benefit from SW HELP gels, but future directions could expand on this work by evaluating the suitability of SW HELP gels in additional biomedical contexts. For example, toward fabricating more complex 3D structures, future studies could explore the use of SW HELP gels in embedded bioprinting.[62] In addition, organoids also undergo lengthy maturation periods and require remodelable matrices to support expansion,[63,64] so SW HELP gels could be explored for the culture of patient-derived organoids. For studies of in vivo regeneration, hydrogel scaffolds must similarly balance sufficient matrix remodeling and local retention to recruit and support cell infiltration.[65,66] As we have already demonstrated the injectability of SW HELP gels, future studies could evaluate their in vivo stability and capacity to support tissue regeneration. Lastly, we envision that spot-welding will be a generalizable approach that can be implemented with a variety of polymers beyond ELP and HA. In particular, for systems that typically undergo considerable swelling, spot-welds could also help prevent erosion due to swelling. Similarly, while here we demonstrated the spot-welding concept using hydrazone bonds, several different types of covalent and physical interactions exist that can be used to create adaptable gels,[4] and the modularity of our platform would support future studies to incorporate these alternative chemistries as spot-welds as well.

In summary, spot-welding offers a simple yet powerful solution to the problem of rapid erosion in dynamic covalent hydrogels, while maintaining their viscoelastic properties. This unique combination makes spot-welded gels highly versatile for diverse applications. Their ability to support cell-mediated matrix remodeling without losing structural integrity is ideal for in vitro human tissue modeling applications. Their injectability opens opportunities for future in vivo applications, and their extrudability and self-healing qualities make them excellent candidates for 3D bioprinting. Overall, this biomaterials strategy holds immense potential to advance both fundamental and translational studies in tissue engineering and regenerative medicine.

■ ASSOCIATED CONTENT

Supporting Information

The Supporting Information is available free of charge at https://pubs.acs.org/doi/10.1021/acs.chemmater.5c02162.

Additional experimental details, including ^{1}H NMR spectra, rheological characterization, viability data, erosion data, and descriptions of Supporting Information videos (PDF)

Supporting Information Video 1 (AVI)

Supporting Information Video 2 (AVI)

■ AUTHOR INFORMATION

Corresponding Author

Sarah C. Heilshorn − *Department of Materials Science and Engineering, Stanford University, Stanford, California 94305, United States;* orcid.org/0000-0002-9801-6304; Email: heilshorn@stanford.edu

Authors

Michelle S. Huang − *Department of Chemical Engineering, Stanford University, Stanford, California 94305, United States; The Institute for Chemistry, Engineering & Medicine for Human Health (Sarafan ChEM-H), Stanford University, Stanford, California 94305, United States;* orcid.org/0000-0002-1814-7786

Renato S. Navarro − *Department of Materials Science and Engineering, Stanford University, Stanford, California 94305, United States; Department of Materials Science and Engineering, University of Florida, Gainesville, Florida 32611, United States;* orcid.org/0000-0001-5949-8251

Lucia G. Brunel − *Department of Chemical Engineering, Stanford University, Stanford, California 94305, United States;* orcid.org/0000-0003-0327-5635

Narelli de Paiva Narciso − *Department of Materials Science and Engineering, Stanford University, Stanford, California 94305, United States*

Giselle Aviles Rodriguez − *Department of Materials Science and Engineering, Stanford University, Stanford, California 94305, United States*

Neil J. Baugh − *Department of Materials Science and Engineering, Stanford University, Stanford, California 94305, United States*

Julien G. Roth − *Institute for Stem Cell Biology and Regenerative Medicine, Stanford University School of Medicine, Stanford, California 94305, United States; Complex In Vitro Systems, Translational Safety, Genentech Inc., South San Francisco, California 94080, United States;* orcid.org/0000-0002-7560-3258

Sarah M. Hull − *Department of Chemical Engineering, Stanford University, Stanford, California 94305, United States*

Kelsea M. Hubka − *Department of Materials Science and Engineering, Stanford University, Stanford, California 94305, United States*

Complete contact information is available at: https://pubs.acs.org/10.1021/acs.chemmater.5c02162

Author Contributions

¶M.S.H. and R.S.N. contributed equally. M.S.H., R.S.N., and S.C.H. conceived and initiated the project. M.S.H. and R.S.N. designed the research, synthesized the materials, conducted the experiments, and analyzed the data. L.G.B. assisted with biomaterials synthesis and the design and execution of the 3D printing experiments. N.P.N. assisted with characterization of ELP modification and hydrogel rheological properties. G.A.R. assisted with biomaterials synthesis. N.J.B. assisted with the

https://doi.org/10.1021/acs.chemmater.5c02162
Chem. Mater. 2025, 37, 9758−9774

hydrogel erosion studies and percolation theory. J.G.R. assisted with cardiomyocyte differentiation and provided guidance on hydrogel design. S.M.H. provided guidance on hydrogel design and preliminary 3D printing experiments. K.M.H. provided guidance on hydrogel design. M.S.H., R.S.N., and S.C.H. wrote the manuscript. S.C.H. supervised the study. All authors edited and approved the manuscript.

Notes

The authors declare the following competing financial interest(s): M.S.H., R.S.N., J.G.R., K.M.H., and S.C.H. are inventors on a patent application (no. 18/489,331) submitted by the Board of Trustees of Stanford University. The authors declare no other competing interests.

■ ACKNOWLEDGMENTS

The authors thank T. Palmer (Stanford Neurosurgery) for providing the iPSCs; F. Galdos (Stanford Institute for Stem Cell Biology and Regenerative Medicine) for helpful discussions regarding cardiomyocyte differentiation; and J. Tok, D. Ruetsche, and J. Oh (Stanford Nano Shared Facilities) for helpful discussions regarding the FTIR methodology. This work was supported by the National Science Foundation (NSF), grants DGE-1656518 (M.S.H., L.G.B., N.J.B., and J.G.R.), CBET-2033302 (S.C.H.), and DMR-2427971 (S.C.H.); the National Institutes of Health (NIH), grants F31-NS132505 (M.S.H.), K99-HL169844 (R.S.N.), F31-EY034785 (L.G.B.), F31-HL175888 (N.J.B.), F31-EY030731 (S.M.H.), R01-HL151997 (S.C.H.), R01-MH137333 (S.C.H.), R01-HL173056 (S.C.H.), and R01-EY035697 (S.C.H.); the Sarafan ChEM-H O'Leary-Thiry Fellowship (M.S.H.); the Gerald J. Lieberman Fellowship (M.S.H. and N.P.N.); the ARCS Foundation Scholarship (L.G.B. and N.J.B.); the American Heart Association, grant 24PRE1191604 (N.P.N.); the PhRMA Foundation Predoctoral Fellowship in Drug Delivery (N.J.B.); the Stanford Bio-X Interdisciplinary Graduate Fellowship (S.M.H.); a Stanford Cardiovascular Institute seed grant (S.C.H.); and a Stanford MCHRI Pediatric IBD seed grant (S.C.H.). Part of this work was performed at the Stanford Nano Shared Facilities (SNSF) RRID:SCR_023230, supported by the NSF under award ECCS-2026822.

■ REFERENCES

(1) Lee, K. Y.; Mooney, D. J. Hydrogels for tissue engineering. *Chem. Rev.* **2001**, *101* (7), 1869−1880.
(2) Khetan, S.; Guvendiren, M.; Legant, W. R.; Cohen, D. M.; Chen, C. S.; Burdick, J. A. Degradation-mediated cellular traction directs stem cell fate in covalently crosslinked three-dimensional hydrogels. *Nat. Mater.* **2013**, *12* (5), 458−465.
(3) Lou, J.; Mooney, D. J. Chemical strategies to engineer hydrogels for cell culture. *Nat. Rev. Chem.* **2022**, *6* (10), 726−744.
(4) Wang, H.; Heilshorn, S. C. Adaptable hydrogel networks with reversible linkages for tissue engineering. *Adv. Mater.* **2015**, *27* (25), 3717−3736.
(5) Rizwan, M.; Baker, A. E. G.; Shoichet, M. S. Designing Hydrogels for 3D Cell Culture Using Dynamic Covalent Crosslinking. *Adv. Healthcare Mater.* **2021**, *10* (12), 2100234.
(6) Chaudhuri, O.; Cooper-White, J.; Janmey, P. A.; Mooney, D. J.; Shenoy, V. B. Effects of extracellular matrix viscoelasticity on cellular behaviour. *Nature* **2020**, *584* (7822), 535−546.
(7) McKinnon, D. D.; Domaille, D. W.; Cha, J. N.; Anseth, K. S. Biophysically defined and cytocompatible covalently adaptable networks as viscoelastic 3D cell culture systems. *Adv. Mater.* **2014**, *26* (6), 865−872.
(8) Rosales, A. M.; Anseth, K. S. The design of reversible hydrogels to capture extracellular matrix dynamics. *Nat. Rev. Mater.* **2016**, *1*, 15012.
(9) Huang, Z.; Delparastan, P.; Burch, P.; Cheng, J.; Cao, Y.; Messersmith, P. B. Injectable dynamic covalent hydrogels of boronic acid polymers cross-linked by bioactive plant-derived polyphenols. *Biomater. Sci.* **2018**, *6* (9), 2487−2495.
(10) Lou, J.; Stowers, R.; Nam, S.; Xia, Y.; Chaudhuri, O. Stress relaxing hyaluronic acid-collagen hydrogels promote cell spreading, fiber remodeling, and focal adhesion formation in 3D cell culture. *Biomaterials* **2018**, *154*, 213−222.
(11) Hull, S. M.; Lou, J.; Lindsay, C. D.; Navarro, R. S.; Cai, B.; Brunel, L. G.; Westerfield, A. D.; Xia, Y.; Heilshorn, S. C. 3D bioprinting of dynamic hydrogel bioinks enabled by small molecule modulators. *Sci. Adv.* **2023**, *9* (13), No. eade7880.
(12) de Paiva Narciso, N.; Navarro, R. S.; Gilchrist, A. E.; Trigo, M. L. M.; Aviles Rodriguez, G.; Heilshorn, S. C. Design parameters for injectable biopolymeric hydrogels with dynamic covalent chemistry crosslinks. *Adv. Healthcare Mater.* **2023**, *12* (27), No. e2301265.
(13) Borelli, A. N.; Young, M. W.; Kirkpatrick, B. E.; Jaeschke, M. W.; Mellett, S.; Porter, S.; Blatchley, M. R.; Rao, V. V.; Sridhar, B. V.; Anseth, K. S. Stress relaxation and composition of hydrazone-crosslinked hybrid biopolymer-synthetic hydrogels determine spreading and secretory properties of MSCs. *Adv. Healthcare Mater.* **2022**, *11* (14), No. e2200393.
(14) Jaeschke, M. W.; Borelli, A. N.; Skillin, N. P.; White, T. J.; Anseth, K. S. Engineering a hydrazone and triazole crosslinked hydrogel for extrusion-based printing and cell delivery. *Adv. Healthcare Mater.* **2024**, *13* (20), No. e2400062.
(15) Weng, L.; Romanov, A.; Rooney, J.; Chen, W. Non-cytotoxic, in situ gelable hydrogels composed of N-carboxyethyl chitosan and oxidized dextran. *Biomaterials* **2008**, *29* (29), 3905−3913.
(16) Zhang, K.; Feng, Q.; Fang, Z.; Gu, L.; Bian, L. Structurally Dynamic Hydrogels for Biomedical Applications: Pursuing a Fine Balance between Macroscopic Stability and Microscopic Dynamics. *Chem. Rev.* **2021**, *121* (18), 11149−11193.
(17) Chen, S.; Liu, A.; Wu, C.; Chen, Y.; Liu, C.; Zhang, Y.; Wu, K.; Wei, D.; Sun, J.; Zhou, L.; et al. Static−dynamic profited viscoelastic hydrogels for motor-clutch-regulated neurogenesis. *ACS Appl. Mater. Interfaces* **2021**, *13* (21), 24463−24476.
(18) Wang, L. L.; Highley, C. B.; Yeh, Y. C.; Galarraga, J. H.; Uman, S.; Burdick, J. A. Three-dimensional extrusion bioprinting of single- and double-network hydrogels containing dynamic covalent crosslinks. *J. Biomed. Mater. Res., Part A* **2018**, *106* (4), 865−875.
(19) Aldana, A. A.; Morgan, F. L. C.; Houben, S.; Pitet, L. M.; Moroni, L.; Baker, M. B. Biomimetic double network hydrogels: Combining dynamic and static crosslinks to enable biofabrication and control cell-matrix interactions. *J. Polym. Sci.* **2021**, *59* (22), 2832−2843.
(20) Li, Y.; Li, T.; Zhu, C.; Li, H.; Fang, R.; Li, R.; Jin, Y.; Zhu, Z.; Xia, L.; Fang, B. Stable-Dynamic Hydrogels Mimicking the Pericellular Matrix for Articular Cartilage Repair. *Adv. Healthcare Mater.* **2025**, *14* (12), 2405081.
(21) Chrisnandy, A.; Blondel, D.; Rezakhani, S.; Broguiere, N.; Lutolf, M. P. Synthetic dynamic hydrogels promote degradation-independent in vitro organogenesis. *Nat. Mater.* **2021**, *21*, 479−487.
(22) Qiao, E.; Fulmore, C. A.; Schaffer, D. V.; Kumar, S. Substrate stress relaxation regulates neural stem cell fate commitment. *Proc. Natl. Acad. Sci. U.S.A.* **2024**, *121* (28), No. e2317711121.
(23) Lee, H. P.; Deo, K. A.; Jeong, J.; Namkoong, M.; Kuan, K. Y.; Tian, L.; Gaharwar, A. K. Injectable, Self-healing, and 3D Printable Dynamic Hydrogels. *Adv. Mater. Interfaces* **2022**, *9* (23), 2201186.
(24) Hefferon, M. E.; Huang, M. S.; Liu, Y.; Navarro, R. S.; de Paiva Narciso, N.; Zhang, D.; Aviles-Rodriguez, G.; Heilshorn, S. C. Cell Microencapsulation Within Engineered Hyaluronan Elastin-Like Protein (HELP) Hydrogels. *Curr. Protoc.* **2023**, *3* (11), No. e917.
(25) Roth, J. G.; Huang, M. S.; Navarro, R. S.; Akram, J. T.; LeSavage, B. L.; Heilshorn, S. C. Tunable hydrogel viscoelasticity

https://doi.org/10.1021/acs.chemmater.5c02162
Chem. Mater. 2025, 37, 9758−9774

modulates human neural maturation. *Sci. Adv.* **2023**, *9* (42), No. eadh8313.
(26) Huang, M. S.; LeSavage, B. L.; Ghorbani, S.; Gilchrist, A. E.; Roth, J. G.; Huerta-López, C.; Mozipo, E. A.; Navarro, R. S.; Heilshorn, S. C. Viscoelastic N-cadherin-like interactions maintain neural progenitor cell stemness within 3D matrices. *Nat. Commun.* **2025**, *16* (1), 5213.
(27) Hunt, D. R.; Klett, K. C.; Mascharak, S.; Wang, H.; Gong, D.; Lou, J.; Li, X.; Cai, P. C.; Suhar, R. A.; Co, J. Y.; et al. Engineered matrices enable the culture of human patient-derived intestinal organoids. *Adv. Sci.* **2021**, *8* (10), 2004705.
(28) Liu, Y.; Gilchrist, A. E.; Johansson, P. K.; Guan, Y.; Deras, J. D.; Liu, Y. C.; Ceva, S.; Huang, M. S.; Navarro, R. S.; Enejder, A.; et al. Engineered Hydrogels for Organoid Models of Human Nonalcoholic Fatty Liver Disease. *Adv. Sci. (Weinh)* **2025**, *12* (22), No. e17332.
(29) LeSavage, B. L.; Zhang, D.; Huerta-López, C.; Gilchrist, A. E.; Krajina, B. A.; Karlsson, K.; Smith, A. R.; Karagyozova, K.; Klett, K. C.; Huang, M. S.; et al. Engineered matrices reveal stiffness-mediated chemoresistance in patient-derived pancreatic cancer organoids. *Nat. Mater.* **2024**, *23* (8), 1138−1149.
(30) LeSavage, B. L.; Suhar, N. A.; Madl, C. M.; Heilshorn, S. C. Production of elastin-like protein hydrogels for encapsulation and immunostaining of cells in 3D. *J. Visualized Exp.* **2018**, *135*, 57739.
(31) Navarro, R. S.; Huang, M. S.; Roth, J. G.; Hubka, K. M.; Long, C. M.; Enejder, A.; Heilshorn, S. C. Tuning polymer hydrophilicity to regulate gel mechanics and encapsulated cell morphology. *Adv. Healthcare Mater.* **2022**, *11* (13), 2200011.
(32) Suhar, R. A.; Huang, M. S.; Navarro, R. S.; Aviles Rodriguez, G.; Heilshorn, S. C. A library of elastin-like proteins with tunable matrix ligands for in vitro 3D neural cell culture. *Biomacromolecules* **2023**, *24* (12), 5926−5939.
(33) Cesaretti, M.; Luppi, E.; Maccari, F.; Volpi, N. A 96-well assay for uronic acid carbazole reaction. *Carbohydr. Polym.* **2003**, *54* (1), 59−61.
(34) Lian, X.; Zhang, J.; Azarin, S. M.; Zhu, K.; Hazeltine, L. B.; Bao, X.; Hsiao, C.; Kamp, T. J.; Palecek, S. P. Directed cardiomyocyte differentiation from human pluripotent stem cells by modulating Wnt/β-catenin signaling under fully defined conditions. *Nat. Protoc.* **2013**, *8* (1), 162−175.
(35) Lee, H.; Kim, B.; Yun, J.; Bae, J.; Park, S.; Jeon, J.; Jang, H. R.; Lee, J.; Lee, S. PIV-MyoMonitor: an accessible particle image velocimetry-based software tool for advanced contractility assessment of cardiac organoids. *Front. Bioeng. Biotechnol.* **2024**, *12*, 1367141.
(36) Pusch, K.; Hinton, T. J.; Feinberg, A. W. Large volume syringe pump extruder for desktop 3D printers. *HardwareX* **2018**, *3*, 49−61.
(37) He, Y.; Yang, F.; Zhao, H.; Gao, Q.; Xia, B.; Fu, J. Research on the printability of hydrogels in 3D bioprinting. *Sci. Rep.* **2016**, *6* (1), 29977.
(38) Ouyang, L.; Yao, R.; Zhao, Y.; Sun, W. Effect of bioink properties on printability and cell viability for 3D bioplotting of embryonic stem cells. *Biofabrication* **2016**, *8* (3), 035020.
(39) Wolf, K. J.; Kumar, S. Hyaluronic acid: incorporating the bio into the material. *ACS Biomater. Sci. Eng.* **2019**, *5* (8), 3753−3765.
(40) Dicker, K. T.; Gurski, L. A.; Pradhan-Bhatt, S.; Witt, R. L.; Farach-Carson, M. C.; Jia, X. Hyaluronan: a simple polysaccharide with diverse biological functions. *Acta Biomater.* **2014**, *10* (4), 1558−1570.
(41) Schanté, C. E.; Zuber, G.; Herlin, C.; Vandamme, T. F. Chemical modifications of hyaluronic acid for the synthesis of derivatives for a broad range of biomedical applications. *Carbohydr. Polym.* **2011**, *85* (3), 469−489.
(42) Straley, K. S.; Heilshorn, S. C. Independent tuning of multiple biomaterial properties using protein engineering. *Soft Matter* **2009**, *5* (1), 114−124.
(43) Urry, D. W.; Gowda, D. C.; Parker, T. M.; Luan, C.-H.; Reid, M. C.; Harris, C. M.; Pattanaik, A.; Harris, R. D. Hydrophobicity scale for proteins based on inverse temperature transitions. *Biopolymers* **1992**, *32* (9), 1243−1250.
(44) Urry, D. W.; Okamoto, K.; Harris, R. D.; Hendrix, C. F.; Long, M. M. Synthetic, crosslinked polypentapeptide of tropoelastin: an anisotropic, fibrillar elastomer. *Biochemistry* **1976**, *15* (18), 4083−4089.
(45) Veronese, F. M. Peptide and protein PEGylation: a review of problems and solutions. *Biomaterials* **2001**, *22* (5), 405−417.
(46) Harris, J. M.; Chess, R. B. Effect of pegylation on pharmaceuticals. *Nat. Rev. Drug Discovery* **2003**, *2* (3), 214−221.
(47) Nischan, N.; Hackenberger, C. P. R. Site-specific PEGylation of proteins: recent developments. *J. Org. Chem.* **2014**, *79* (22), 10727−10733.
(48) Staros, J. V. N-hydroxysulfosuccinimide active esters: bis(N-hydroxysulfosuccinimide) esters of two dicarboxylic acids are hydrophilic, membrane-impermeant, protein cross-linkers. *Biochemistry* **1982**, *21* (17), 3950−3955.
(49) Staros, J. V.; Wright, R. W.; Swingle, D. M. Enhancement by N-hydroxysulfosuccinimide of water-soluble carbodiimide-mediated coupling reactions. *Anal. Biochem.* **1986**, *156* (1), 220−222.
(50) Richardson, B. M.; Wilcox, D. G.; Randolph, M. A.; Anseth, K. S. Hydrazone covalent adaptable networks modulate extracellular matrix deposition for cartilage tissue engineering. *Acta Biomater.* **2019**, *83*, 71−82.
(51) Madl, C. M.; Heilshorn, S. C. Rapid Diels−Alder cross-linking of cell encapsulating hydrogels. *Chem. Mater.* **2019**, *31* (19), 8035−8043.
(52) Cho, S.; Lee, C.; Skylar-Scott, M. A.; Heilshorn, S. C.; Wu, J. C. Reconstructing the heart using iPSCs: Engineering strategies and applications. *J. Mol. Cell. Cardiol.* **2021**, *157*, 56−65.
(53) Buikema, J. W.; Lee, S.; Goodyer, W. R.; Maas, R. G.; Chirikian, O.; Li, G.; Miao, Y.; Paige, S. L.; Lee, D.; Wu, H.; et al. Wnt Activation and Reduced Cell-Cell Contact Synergistically Induce Massive Expansion of Functional Human iPSC-Derived Cardiomyocytes. *Cell Stem Cell* **2020**, *27* (1), 50−63.
(54) Slotvitsky, M. M.; Tsvelaya, V. A.; Podgurskaya, A. D.; Agladze, K. I. Formation of an electrical coupling between differentiating cardiomyocytes. *Sci. Rep.* **2020**, *10* (1), 7774.
(55) Eng, G.; Lee, B. W.; Protas, L.; Gagliardi, M.; Brown, K.; Kass, R. S.; Keller, G.; Robinson, R. B.; Vunjak-Novakovic, G. Autonomous beating rate adaptation in human stem cell-derived cardiomyocytes. *Nat. Commun.* **2016**, *7* (1), 10312.
(56) Lee, S.; Serpooshan, V.; Tong, X.; Venkatraman, S.; Lee, M.; Lee, J.; Chirikian, O.; Wu, J. C.; Wu, S. M.; Yang, F. Contractile force generation by 3D hiPSC-derived cardiac tissues is enhanced by rapid establishment of cellular interconnection in matrix with muscle-mimicking stiffness. *Biomaterials* **2017**, *131*, 111−120.
(57) Morgan, F. L. C.; Moroni, L.; Baker, M. B. Dynamic Bioinks to Advance Bioprinting. *Adv. Healthcare Mater.* **2020**, *9* (15), 1901798.
(58) Dinkgreve, M.; Paredes, J.; Denn, M. M.; Bonn, D. On different ways of measuring "the" yield stress. *J. Non-Newtonian Fluid Mech.* **2016**, *238*, 233−241.
(59) Barnes, H. A. *A Handbook of Elementary Rheology*; University of Wales: Aberystwyth, 2000.
(60) Habib, A.; Sathish, V.; Mallik, S.; Khoda, B. 3D Printability of Alginate-Carboxymethyl Cellulose Hydrogel. *Materials (Basel)* **2018**, *11* (3), 454.
(61) Seymour, A. J.; Shin, S.; Heilshorn, S. C. 3D printing of microgel scaffolds with tunable void fraction to promote cell infiltration. *Adv. Healthcare Mater.* **2021**, *10* (18), No. e2100644.
(62) Brunel, L. G.; Hull, S. M.; Heilshorn, S. C. Engineered assistive materials for 3D bioprinting: support baths and sacrificial inks. *Biofabrication* **2022**, *14* (3), 032001.
(63) Kratochvil, M. J.; Seymour, A. J.; Li, T. L.; Paşca, S. P.; Kuo, C. J.; Heilshorn, S. C. Engineered materials for organoid systems. *Nat. Rev. Mater.* **2019**, *4* (9), 606−622.
(64) Huang, M. S.; Christakopoulos, F.; Roth, J. G.; Heilshorn, S. C. Organoid bioprinting: from cells to functional tissues. *Nat. Rev. Bioeng.* **2025**, *3* (2), 126−142.

(65) Mao, A. S.; Mooney, D. J. Regenerative medicine: Current therapies and future directions. *Proc. Natl. Acad. Sci. U.S.A.* **2015**, *112* (47), 14452−14459.
(66) Zhao, X.; Sun, X.; Yildirimer, L.; Lang, Q.; Lin, Z. Y.; Zheng, R.; Zhang, Y.; Cui, W.; Annabi, N.; Khademhosseini, A. Cell infiltrative hydrogel fibrous scaffolds for accelerated wound healing. *Acta Biomater.* **2017**, *49*, 66−77.

https://doi.org/10.1021/acs.chemmater.5c02162
Chem. Mater. 2025, 37, 9758−9774